PLOS PATHOGENS

RESEARCH ARTICLE

The pneumococcal two-component system SirRH is linked to enhanced intracellular survival of *Streptococcus pneumoniae* in influenza-infected pulmonary cells

Nicolás M. Reinoso-Vizcaíno[1], Melina B. Cian[1,2], Paulo R. Cortes[1], Nadia B. Olivero[1], Mirelys Hernandez-Morfa[1], Germán E. Piñas[1,3], Chandan Badapanda[4], Ankita Rathore[4], Daniel R. Perez[5], José Echenique[1]*

1 Departamento de Bioquímica Clínica—CIBICI (CONICET), Facultad de Ciencias Químicas, Universidad Nacional de Córdoba, Córdoba, Argentina, **2** Department of Microbiology and Immunology, Health Sciences Center, University of Oklahoma, Oklahoma, United States of America, **3** School of Biological Sciences, University of Utah, Salt Lake City, Utah, United States of America, **4** Bioinformatics Division, Xcelris Labs Limited, Ahmedabad, India, **5** Department of Population Health, College of Veterinary Medicine, University of Georgia, Athens, Georgia, United States of America

* jeche@fcq.unc.edu.ar.

OPEN ACCESS

Citation: Reinoso-Vizcaíno NM, Cian MB, Cortes PR, Olivero NB, Hernandez-Morfa M, Piñas GE, et al. (2020) The pneumococcal two-component system SirRH is linked to enhanced intracellular survival of *Streptococcus pneumoniae* in influenza-infected pulmonary cells. PLoS Pathog 16(8): e1008761. https://doi.org/10.1371/journal.ppat.1008761

Editor: Carlos Javier Orihuela, The University of Alabama at Birmingham, UNITED STATES

Received: September 18, 2019

Accepted: June 29, 2020

Published: August 13, 2020

Data Availability Statement: All relevant data are within the paper and its Supporting Information files.

Funding: This work was founded by the National Council of Scientific and Technological Research (PIP-CONICET 2012, to JE); by the National Agency of Scientific and Technological Promotion (ANPCYT; FONCYT PICT 2012 #2840- Prestamo BID, to JE; FONCYT PICT 2016 #0805-Prestamo

Abstract

The virus-bacterial synergism implicated in secondary bacterial infections caused by *Streptococcus pneumoniae* following infection with epidemic or pandemic influenza A virus (IAV) is well documented. However, the molecular mechanisms behind such synergism remain largely ill-defined. In pneumocytes infected with influenza A virus, subsequent infection with *S. pneumoniae* leads to enhanced pneumococcal intracellular survival. The pneumococcal two-component system SirRH appears essential for such enhanced survival. Through comparative transcriptomic analysis between the Δ*sirR* and *wt* strains, a list of 179 differentially expressed genes was defined. Among those, the *clpL* protein chaperone gene and the *psaB* Mn^{+2} transporter gene, which are involved in the stress response, are important in enhancing *S. pneumoniae* survival in influenza-infected cells. The Δ*sirR*, Δ*clpL* and Δ*psaB* deletion mutants display increased susceptibility to acidic and oxidative stress and no enhancement of intracellular survival in IAV-infected pneumocyte cells. These results suggest that the SirRH two-component system senses IAV-induced stress conditions and controls adaptive responses that allow survival of *S. pneumoniae* in IAV-infected pneumocytes.

Author summary

S. pneumoniae is an inhabitant of the human nasopharynx that is capable of causing a variety of infections contributing to an estimated 1.6 million deaths each year. Many of these deaths occur as result of secondary *S. pneumoniae* infections following seasonal or pandemic influenza. Although *S. pneumoniae* is considered a typical extracellular pathogen, an intracellular survival mechanism has been more recently recognized as significant

BID, to JE), the Scientific and Technological Secretary of the National University of Cordoba (SECYT-UNC 2018/2019, to JE) and by funds from NIAID-Center of Excellence for Influenza Research and Surveillance - Option 15B HHSN272201400008C (to DRP and JE). NRV and NO had PhD fellowships from CONICET. MHM had fellowships from ANPCYT. JE is a member of the Research Career of CONICET. The funders had no role in study design, data collection and analysis, decision to publish, or preparation of the manuscript.

Competing interests: The authors have declared that no competing interests exist.

in bacterial pathogenesis. The synergistic effects between influenza A and *S. pneumoniae* in secondary bacterial infection are well documented; however, the effects of influenza infections on intracellular survival of *S. pneumoniae* are ill-defined. Here, we provide evidence that influenza infection increases *S. pneumoniae* intracellular survival in pneumocytes. We demonstrate that the poorly understood SirRH signal transduction system in pneumococcus controls the expression of genes involved in the stress response that *S. pneumoniae* needs to increase intracellular survival in influenza A-infected pneumocytes. These findings have important implications for understanding secondary bacterial pathogenesis following influenza and for the treatment of such infections in influenza-stricken patients.

Introduction

The World Health Organization (WHO) estimates that seasonal influenza virus infections result in about 1 billion infections, 3 to 5 million cases of severe disease, and between 300,000 and 500,000 deaths around the world every year. Oftentimes, influenza infections are complicated by secondary bacterial infections, particularly caused by *S. pneumoniae*. About 11–35% of laboratory-confirmed cases of influenza infection are associated with secondary *S. pneumoniae* infections [1]. Such secondary infections ultimately exacerbate the severity of respiratory symptoms resulting in excess morbidity and mortality [2, 3]. Highlighting the importance of *S. pneumoniae*, it has been proposed that the majority of 40–50 million deaths during the 1918 Spanish influenza pandemic were associated to *S. pneumoniae* secondary bacterial infections [4, 5]. The *S. pneumoniae* is a Gram-positive bacterium of great significance on human health, being the causal agent of otitis, sinusitis, as well as severe diseases such as community-acquired pneumonia, sepsis, and meningitis [6]. More recently, about 34% of the deaths associated with the 2009 pandemic influenza were also linked to secondary bacterial infections, with *S. pneumoniae* as the most commonly associated bacterial pathogen (in addition to *Staphylococcus aureus* and *Streptococcus pyogenes)* [7, 8].

A myriad of concomitant events and factors are thought to be associated with the promotion of secondary bacterial infections following infection with influenza virus: 1) influenza infections produce damage of pulmonary epithelial cells, decreasing the mucocilliary clearance and favoring bacterial adherence and infection [9]; 2) the virus' neuraminidase results in the desialylation of mucins, which increases pneumococcal adherence [10]; and 3) macrophages and neutrophils infected with influenza virus show impaired phagocytosis of pneumococci [11]. Although these and perhaps other virus-induced modifications on different host cells and tissues [1–3, 8, 12] can contribute to secondary *S. pneumoniae* infections, the precise molecular mechanisms of synergism between influenza viruses and *S. pneumoniae* remain poorly understood.

S. pneumoniae is considered a typical extracellular pathogen. However, mounting evidence suggests a significant role in the replication and survival of *S. pneumoniae* inside host cells for disease progression and pathogenesis. In this regard, Ercoli *et al* [13] described that intracellular replication of *S. pneumoniae* in splenic macrophages acts as a bacterial reservoir for septicemia. Ogawa *et al* [14] characterized autophagic vesicles that contain pneumococci during the first hours of bacterial infection of human nasopharyngeal epithelial cells and mouse embryonic fibroblasts. The same work also showed that the bacterial protein Ply, a cholesterol-binding, thiol-activated cytolysin, provides advantages for the bacteria to escape from endosomal elimination at the early stages of infection. We previously reported that the two-component

systems (TCSs) ComDE and CiaRH are involved in the pneumococcal stress response to acidic conditions and the intracellular survival of *S. pneumoniae* in pneumocytes [15]. In addition, we recently reported that the crosstalk signaling between the serine/threonine kinase StkP and ComE controls H_2O_2 production in *S. pneumoniae* modulating its intracellular survival in pneumocytes [16].

In this report, we studied how IAV infection affects the intracellular survival of *S. pneumoniae* in an in vitro pneumocyte IAV-*S. pneumoniae* superinfection model. We observed that *S. pneumoniae* exhibits increased intracellular survival in IAV-infected cells. In *S. pneumoniae*, we identified the two-component system SirRH as a mediator of such increased survival. We found that SirRH controls the expression of 179 pneumococcal genes, such as *clpL* and *psaB*, which encode a molecular chaperone and a Mn^{+2} transporter, respectively. We show that *clpL* and *psaB* expression is required in response to acidic and oxidative stress and for bacterial survival in IAV-infected pneumocytes.

Results

Enhanced intracellular survival of *S. pneumoniae* in influenza virus-infected pneumocytes

We previously demonstrated that the *S. pneumoniae* R801 strain, considered in this work as the wild-type (*wt*) strain, can survive inside pneumocytes for several hours [16]. To further define whether a concomitant influenza virus infection would affect *S. pneumoniae* intracellular survival, we established an in vitro IAV-*S. pneumoniae* superinfection model in human-derived A549 pneumocyte cells. As a model virus, we utilized the laboratory-adapted influenza A/Puerto Rico/8/1934 (H1N1) virus (IAV), which readily infects and replicates in A549 cells [17]. IAV at a multiplicity of infection (MOI) of either 1, 5, or 10 (S1A Fig) was used to inoculated A549 cells. Virus replication was allowed to progress for 24 h before infection with the *S. pneumoniae* R801 strain at a MOI of 30. Flow cytometry using Annexin-V-ACP/PI labeling to test necrosis/apoptosis levels revealed that a MOI of 10 of IAV led to ~5% increase in the number of necrotic/apoptotic cells compared to non-infected cells (S1A Fig) and ~15% after bacterial superinfection using a bacterial MOI of 30 (S1B Fig), as described [16]. In further studies, we used IAV at a MOI of 10 and *S. pneumoniae* at a MOI of 30 in the superinfection model. Gentamicin was used to eliminate extracellular bacteria before the evaluation of intracellular *S. pneumoniae* following the classical protection assay [16]. Prior IAV inoculation consistently increased bacterial survival by ~2 fold in A549 pneumocytes (Fig 1A, S2A and S2B Fig).

We determined that this synergism requires active viral infection, because when we co-infected with the same viral MOI but using heat-inactivated IAV, we observed the same level of bacterial intracellular survival than non-virus infected cells (S1C Fig).

The pneumococcal R801 strain is a derivative of the R6 strain [18]. To determine if increased survival in IAV-infected cells was bacterial strain-dependent, we tested the intracellular survival of the non-encapsulated R6 strain itself (derived from the serotype 2 clinical isolate D39) [19, 20] and another non-encapsulated D39 (D39 *cpsB*::*spc*) strain (S1 Table). The R6 and D39 *cpsB*::*spc* strains behaved as the R801 strain in IAV-infected A549 cells (S3 Fig). These studies suggest that increased intracellular bacterial survival in IAV-infected cells is independent of the bacterial strain.

Since human bronchial epithelial cells are one of the major targets for IAV infection, we decided to carry out our model in this type of cell. [21]. We used human bronchial cells immortalized with the origin-of-replication defective SV40 plasmid, a cell line known as 16HBE14o- [22]. We observed a significant increase in the bacterial intracellular survival in these IAV-infected cells, as in A549 cells. The same phenotype was reproduced using the cell

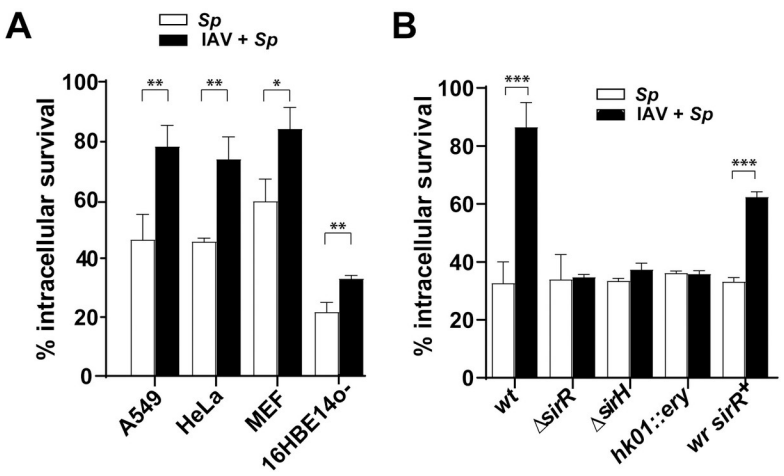

Fig 1. Enhancement of pneumococcal intracellular survival by influenza A infection is mediated by the SirRH two-component system. (A) The IAV-*S. pneumoniae* synergism is independent of the cell line. The A549, MEF, 16HBE14o- and HeLa cells were treated for 24 h with a viral MOI of 10 and posteriorly infected with the pneumococcal *wt* strain using a bacterial MOI of 30. Bacterial survival progression was monitored using a typical protection assay. Survival percentages were calculated by considering the total amount of internalized bacteria after 30 min of extracellular antibiotic treatment as representing 100% for each strain. After antibiotic treatment, samples were taken at 4 hours, and pneumocytes were lysed to release pneumococci. Samples were diluted in BHI, spread on BHI-blood-agar plates and incubated at 37˚C for 16 h. IAV-infected cells are indicated with black bars and non-virus infected cells with white bars. (B) The synergism between IAV and *S. pneumoniae* is mediated by the SirRH two-component system. A549 cells were previously infected with a viral MOI of 10 for 24 h, and then coinfected by the *wt*, Δ*sirH*, *hk01*::ery (or *sirH*::*ery*) and Δ*sirR* strains, and the revertant of the Δ*sirR* mutant (*wr sirR*$^+$). Intracellular survival rates were determined as described in panel A. IAV-infected cells are indicated with black bars and non-virus infected cells with white bars. For both panels, data are representative of at least three independent experiments and statistically significant differences are indicated as $p<0.05$ (*), $p<0.01$ (**) or $p<0.001$ (***).

https://doi.org/10.1371/journal.ppat.1008761.g001

mouse embryonic fibroblasts (MEF) and cervical cancer cells (HeLa) (Fig 1A, S2A Fig), suggesting that this phenomenon is cell-line independent.

The SirRH two-component system mediates enhanced pneumococcal survival in influenza-infected cells

S. pneumoniae requires ComE and CiaR response regulators to control the acid stress response and intracellular survival in non-IAV infected A549 pneumocytes [15, 16]. We hypothesized that pneumococcal two-component systems (TCSs) sense physiological changes induced by IAV-infection of pneumocytes and mediate adaptative responses that lead to increased intracellular bacterial survival. Next, we considered that the intracellular changes induced by IAV-infection generate stress conditions sensed by *S. pneumoniae* via TCSs other than ComE and CiaR [15, 16]. From a previous systematic screening of insertion-duplication histidine kinase (*hk*) mutants of *S. pneumoniae* [15] (S1 Table), we focused the search on *hk* mutations that were null for pneumococcal intracellular survival in the absence of IAV infection. When non-IAV infected A549 pneumocytes were inoculated with the *S. pneumoniae hk* mutants, most of them showed no changes in intracellular survival compared to the *wt* strain, including the *hk01*::*ery* mutant (S4 Fig). However, in the context of IAV infection, the *hk01*::*ery* mutant showed impaired pneumococcal intracellular survival compared to the *wt* strain (Fig 1B), suggesting that their components participate in sensing the IAV-infected environment. The *hk01*::*ery* mutant corresponds to TCS01, one of the least studied TCSs but previously identified as a virulent factor in *S. pneumoniae* [23–25]. TCS01, hereafter named SirRH (for stress-induced response), contains the SirH histidine kinase and the SirR response regulator. Deletion

mutants for the *sirR* (*ΔsirR*) and *sirH* (*ΔsirH*) genes obtained using the Janus cassette [26] (S1 Table), showed similar impairment in intracellular survival as the *hk01*::*ery* mutant compared to the *wt* strain in IAV-infected A549 pneumocytes (Fig 1B). In contrast, the reconstructed revertant of the Δ*sirR* mutant (*wr sirR*$^{+}$) recovered the *wt*-like phenotype (Fig 1B). These results confirmed that *S. pneumoniae* needs SirRH for increased intracellular survival in IAV-infected A549 pneumocytes.

SirRH participates in the acidic stress response of *S. pneumoniae*

S. pneumoniae requires an adequate acidic stress response for intracellular survival in pneumocytes [15, 16] and survives in acidic autophagic vesicles of Detroit 562 human nasopharyngeal epithelial cells and mouse embryonic fibroblasts (MEFs) [14]. In IAV-infected cells, *S. pneumoniae* is likely to survive in acidic autophagic vesicles, which implies exposure to the acidic environment and increased ROS production induced by IAV [14]. Since bacterial TCSs typically respond to changes in environmental conditions, we hypothesized that SirRH senses IAV-induced physiological changes at the intracellular level, resulting in an adaptive stress response that improves *S. pneumoniae* survival in autophagic vesicles in IAV-infected pneumocytes [27]. The Δ*sirR* mutant was incubated in culture media at pH 4.8 showing a 10^3-fold decrease in bacterial cell viability compared to the *wt*. In contrast, the *wr sirR*$^{+}$ revertant recovered the acidic tolerance (Fig 2A).

The Δ*sirR* mutant behaved similarly as the control *atpC*^{A49T} mutant (Fig 2A), which contains a point mutation at position 49 of the subunit ε of the $F_0.F_1$-ATPase (a proton pump that controls intracellular pH) and is unable to respond to acidic stress in acidified media [15, 28]. These results suggest that SirRH is required for the acidic stress response of *S. pneumoniae*. To further define the role of vesicle acidification in *S. pneumoniae* survival, A549 cells were treated with Bafilomycin A1, a known v-ATPase inhibitor that halts lysosomal acidification [29] and prevents the fusion between endosome/autophagosome and lysosome, and simultaneously inoculated with *S. pneumoniae*. Intracellular survival of the pneumococcal *wt* strain showed a significant increase when A549 cells were exposed to Bafilomycin A1 (Fig 2B, S5 Fig), as described [30]. In contrast, when Bafilomycin A1-treated or non-treated A549 pneumocytes were infected with either the control *atpC*^{A49T} mutant or the Δ*sirR* mutant cells, *S. pneumoniae* showed no increased survival (Fig 2B, S5 Fig) suggesting that the Δ*sirR* mutant is unable to respond to the pH variation in vesicles. It must be noted that Bafilomycin A1 does not affect the growth of any of these strains in bacterial growth medium (S6 Fig). To further establish the association between IAV infection and pneumococci contained in acidic vesicles, IAV/*S. pneumoniae*-infected A549 cells were stained with Lysotracker Deep Red, a cell-permeable dye that targets acidic organelles in the lysosomes.

Confocal microscopy revealed acidic vesicles (red by Lysotracker staining) containing pneumococci (blue by DAPI staining) (Fig 2C and 2D). IAV infection led to about half reduction in pneumococci-containing acidic vesicles compared to mock-infected cells (Fig 2E), consistent with IAV's-induced inhibition of the autophagosome/lysosome fusion step [31]. The reduced presence of bacterial cells in autolysosomes explains, at least in part, the increased intracellular survival of *Sp* in IAV-infected cells. Thus, SirRH is likely involved in the regulation of stress genes required for pneumococcal adaptation to IAV-induced acidic stress conditions.

SirRH is involved in the oxidative stress response of *S. pneumoniae*

We previously reported that the StkP/ComE pathway is involved in the regulation of the oxidative stress response that affects the intracellular survival of *S. pneumoniae* in pneumocytes

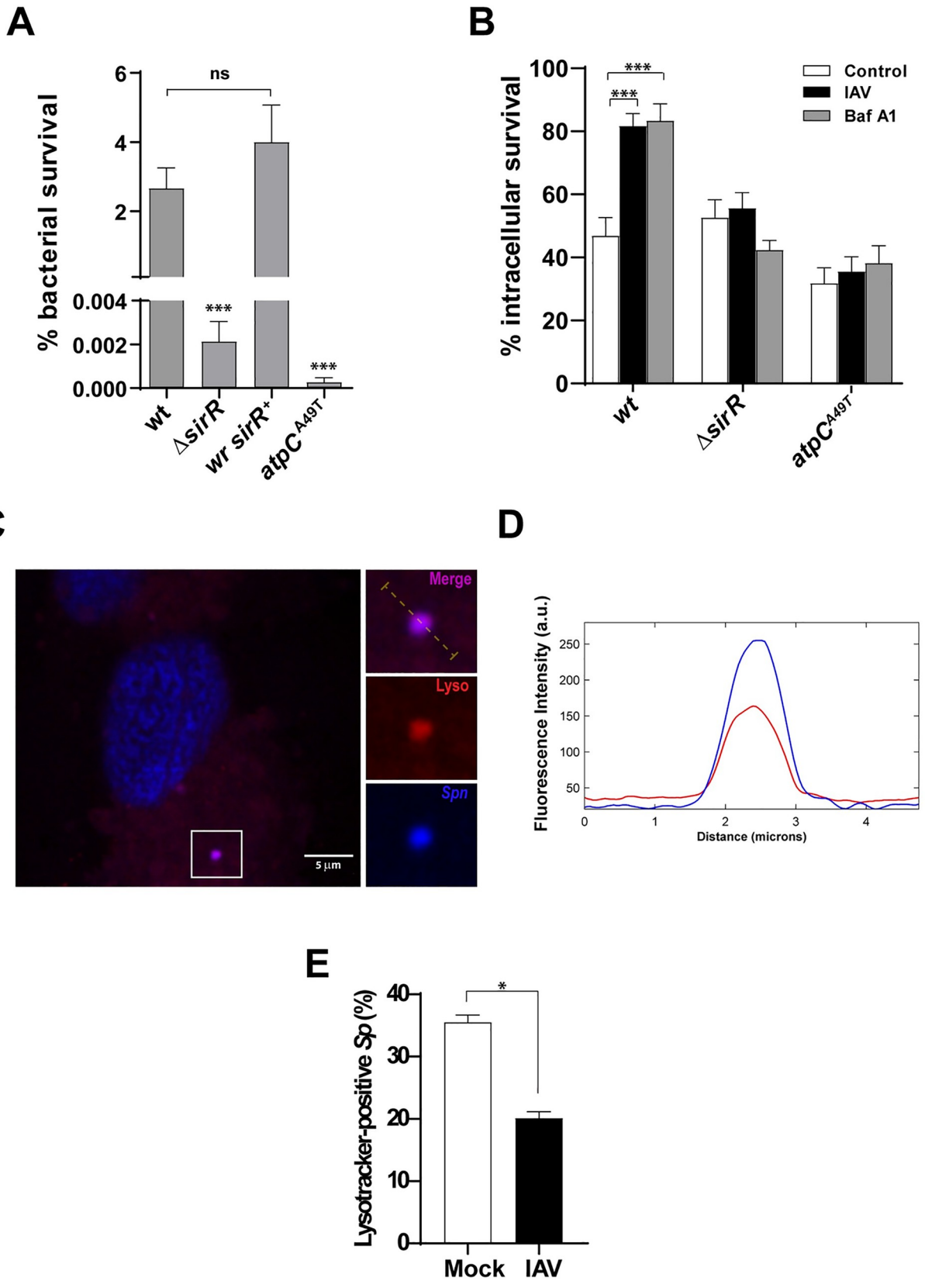
A
% bacterial survival
6
4
2
0.004
0.002
0.000
ns
***
***
wt
ΔsirR
wr sirR+
atpCA49T
B
% intracellular survival
100
80
60
40
20
0
***
***
Control
IAV
Baf A1
wt
ΔsirR
atpCA49T
C
Merge
Lyso
Spn
5 µm
D
Fluorescence Intensity (a.u.)
250
200
150
100
50
0
1
2
3
4
Distance (microns)
E
Lysotracker-positive Sp (%)
40
30
20
10
0
*
Mock
IAV

Fig 2. SirRH controls the acidic stress response of *S. pneumoniae* in both culture media and pneumocytes. (A) The Δ*sirR* mutant is susceptible to acidified media. The Δ*sirR*, *wr sirR*$^{+}$, *atpC*^{A49T} and *wt* cells were grown in BHI until an OD_{620nm} 0.3 and then incubated in ABM at pH 4.8 for 1 h. Viable cells were assessed by spreading dilutions in BHI-blood-agar plates and incubating these at 37˚C for 16 h. (B) Bafilomycin-A1-induced lysosomal neutralization does not affect the impaired intracellular survival of *the ΔsirR mutant* in IAV-infected cells. A549 cells were infected with the Δ*sirR*, *atpC*^{A49T} and *wt* cells and intracellular survival was determined as described in the Fig 1. White bars correspond to non-virus infected cells, black bars to IAV-infected cells and gray bars to Bafilomycin-A1-treated cells. (C) IAV-infected A549 cells showed a diminished percentage of *S. pneumoniae* colocalizing with lysosomes. Representative confocal micrograph showing colocalization of *S. pneumoniae* (dyed with DAPI) with acidic vesicles dyed with Lysotracker Deep Red in A549 cells. IAV-infected and mock-infected A549 cells were posteriorly infected with *S. pneumoniae* for 3 h, and stained with the acidotropic LysoTracker Deep Red dye. The event showed in this panel was localized at z-stack no.21 (out of 35). Scale bar, 5 μm. (D) *S. pneumoniae* colocalize with acidic vesicles in A549 cells. Multichannel plot profile corresponding to the yellow line in the merge inset in "a" depict the fluorescent intensities (a.u., arbitrary units) of LysoTracker Deep Red and DAPI-stained *S. pneumoniae* (blue). (E) Quantification of LysoTracker association with DAPI-stained *S. pneumoniae* in mock-infected and IAV-infected A549 cells at 3 hpi with pneumococci. White bar corresponding to mock-infected cells and gray bar to IAV-infected cells. n ≥ 100 bacteria per coverslip. Values represent the mean ± SEM of at least three replicates. Statistical significance was calculated by Student´s t-test (*; $p<0.05$).

https://doi.org/10.1371/journal.ppat.1008761.g002

[16]. Additionally, previous reports had indicated that the oxidative stress response is controlled by TCS04 [32], suggesting a complex regulatory system that likely involves the participation of other signal transduction systems. To test the putative role of SirRH in the oxidative stress response of *S. pneumoniae*, we examined the hydrogen peroxide resistance of the Δ*sirR* mutant (20 mM H_2O_2 in BHI media for 1 h), which was reduced by approximately 30 times while the *wr sirR*$^{+}$ (revertant) displayed a hydrogen peroxide resistance similar to *wt* (Fig 3A).

As a control, we tested the Δ*sodA* mutant (S1 Table), a strain deficient in the oxidative stress response that displayed a 10-fold decrease in H_2O_2 resistance compared to the *wt* (Fig 3A) [33, 34]. These observations suggest a role of SirRH in the oxidative stress response. Since IAV-infection of A549 cells leads to enhanced reactive oxygen species (ROS) production and alteration of the antioxidant defense [35, 36], we measured the intracellular ROS levels using

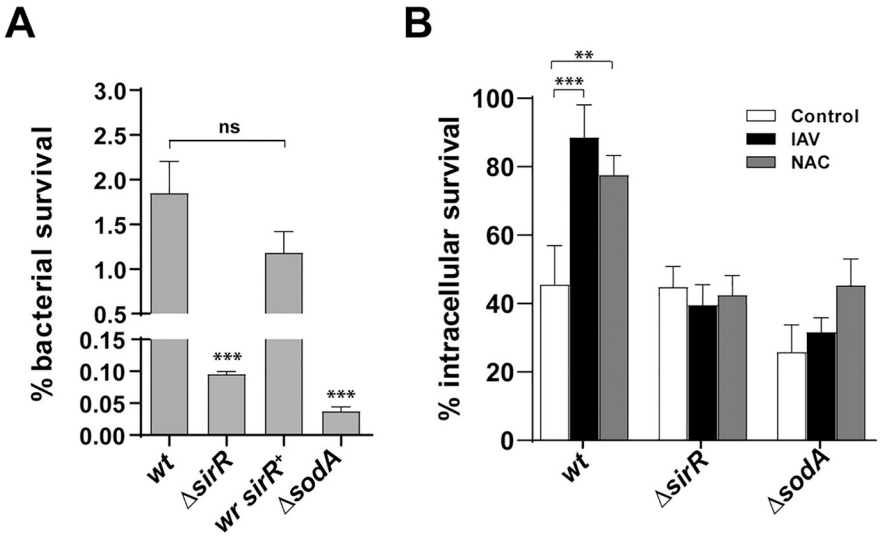

Fig 3. SirRH controls the oxidative stress response of *S. pneumoniae* in both culture media and pneumocytes. (A) The Δ*sirR* mutant is sensitive to H_2O_2. The Δ*sirR*, *wr sirR*$^{+}$, Δ*sodA* and *wt* cells were grown in BHI and then exposed at BHI medium containing 20 mM H_2O_2 for 2 h. After that, viable cells were determined by spreading dilutions in BHI-blood-agar plates and incubating these at 37˚C for 16 h. (B) Inhibition of ROS production in A549 cells does not affect the intracellular survival of *the ΔsirR mutant*. A549 cells were infected with the Δ*sirR*, Δ*sodA* and *wt* cells and intracellular survival was determined as described in the Fig 1 legend. White bars correspond to non-virus infected cells, black bars to IAV-infected cells and gray bars to NAC-treated cells. For all panels, data are representative of at least three independent experiments and statistically significant differences are indicated as $p<0.05$ (*) or $p<0.001$ (***).

https://doi.org/10.1371/journal.ppat.1008761.g003

H_2DCF-DA. ROS production increased by 33% in IAV-infected cells compared to mock-infected cells (S8 Fig). These results suggest that reduced ROS resistance is likely responsible for the reduced intracellular survival of the Δ*sirR*, and Δ*sodA* mutants in IAV-infected A549 cells (Fig 3B, S7 Fig). To further explore the effects of ROS production on the intracellular survival mechanism of *S. pneumoniae*, A549 cells were treated with 5 mM N-acetyl-L-cysteine (NAC), a potent ROS inhibitor [37], at the same time of *S. pneumoniae* inoculation (S9 Fig). In the absence of IAV infection, the NAC-treated A549 cells lead to increased survival of the *S. pneumoniae wt* strain (~2-fold) compared to non-NAC-treated A549 cells.

In contrast, the Δ*sirR* and Δ*sodA* mutants were less sensitive to the effects of low ROS biosynthesis (inhibited by NAC) (Fig 3B, S7 Fig). Of note, NAC had no effect on the growth of bacterial strains in vitro (S10 Fig). Overall, SirRH likely senses ROS production to activate an oxidative stress response that allows *S. pneumoniae* to survive into autophagosomes.

SirR regulates expression of pneumococcal stress genes

Bacterial response regulators control gene expression to develop an adaptive response to stress conditions [27]. To identify the SirR-regulated genes, we compared the transcriptomes of the Δ*sirR* and *wt* strains by RNAseq analysis. These strains were grown in acidified media at the exponential growth phase, and total RNA was purified and analyzed as described [16]. The transcriptomic analysis revealed the differential expression of 179 genes, 65 were down-regulated and 114 were up-regulated (Fig 4A).

A scatter plot (S11A Fig) and a volcano plot (S11B Fig) summarize the data obtained from these analyses (S2 Table). We identified that SirR controls, directly or indirectly, the expression of stress genes such as those coding for molecular chaperones, redox homeostasis, as well as genes involved in cation and metabolite transport, cell wall biosynthesis, amino acid biosynthesis, purine/pyrimidine, central metabolism, ribosomal and translation structures, among others (Fig 4B). The expression of *sirH* showed a 3-fold decrease in the Δ*sirR* mutant, suggesting that the SirRH TCS is auto-regulating its own genes (Fig 4C).

We focused on stress genes and confirmed by RT-qPCR that in the Δ*sirR* mutant there was decreased expression of *sirH* (17.9 fold), *clpL* (3.9 fold) and *psaB* (2.4 fold), and increased transcription of *murN* (2.3 times), *glyA* (3.2 times), and *aroC* (3 times) compared to the *wt* strain (Fig 4C). The *clpL* gene encodes for a molecular chaperone (heat shock protein) involved in stress response [38, 39], *murN* encodes for an enzyme of cell-wall biosynthesis [40], *glyA* encodes for a glycine hydroxymethyltransferase [41], *psaB* encodes for a subunit of a manganese ABC transporter related to oxidative resistance [32, 34], and *aroC* encodes for chorismate synthase involved in aromatic amino acid biosynthesis in bacteria [42].

The proteomes of the Δ*sirR* and the *wt* strains were also compared using protein extracts obtained from bacterial cells grown at pH 5.9 (same conditions as for RNAseq assays). By LC-MS/MS, we detected 925 proteins in total, we found differential expression of 33 down-regulated and 33 up-regulated proteins. Lack of SirR expression in the Δ*sirR* mutant was confirmed in these analyses (Fig 5A).

The full list of differentially expressed proteins at pH 5.9 is available (S3 Table). When these data were compared with those obtained by RNAseq analysis, we obtained a correlation between the expression of the *clpL*, *psaB*, *dpr* (codes for iron-containing ferritin) [43], *trxA* (codes for thioredoxin) [44], *groES* (codes for molecular chaperones) [45], and *nrdD* (codes for ribonucleotide reductase) [46] genes with the expression of their corresponding encoded proteins (Fig 5B). Of note, the expression of known stress response proteins ClpL and PsaB [34, 39] was repressed in the Δ*sirR* mutant. To further explore whether differences in protein expression was due to the altered sensitivity of the Δ*sirR* mutant to acidic stress conditions or

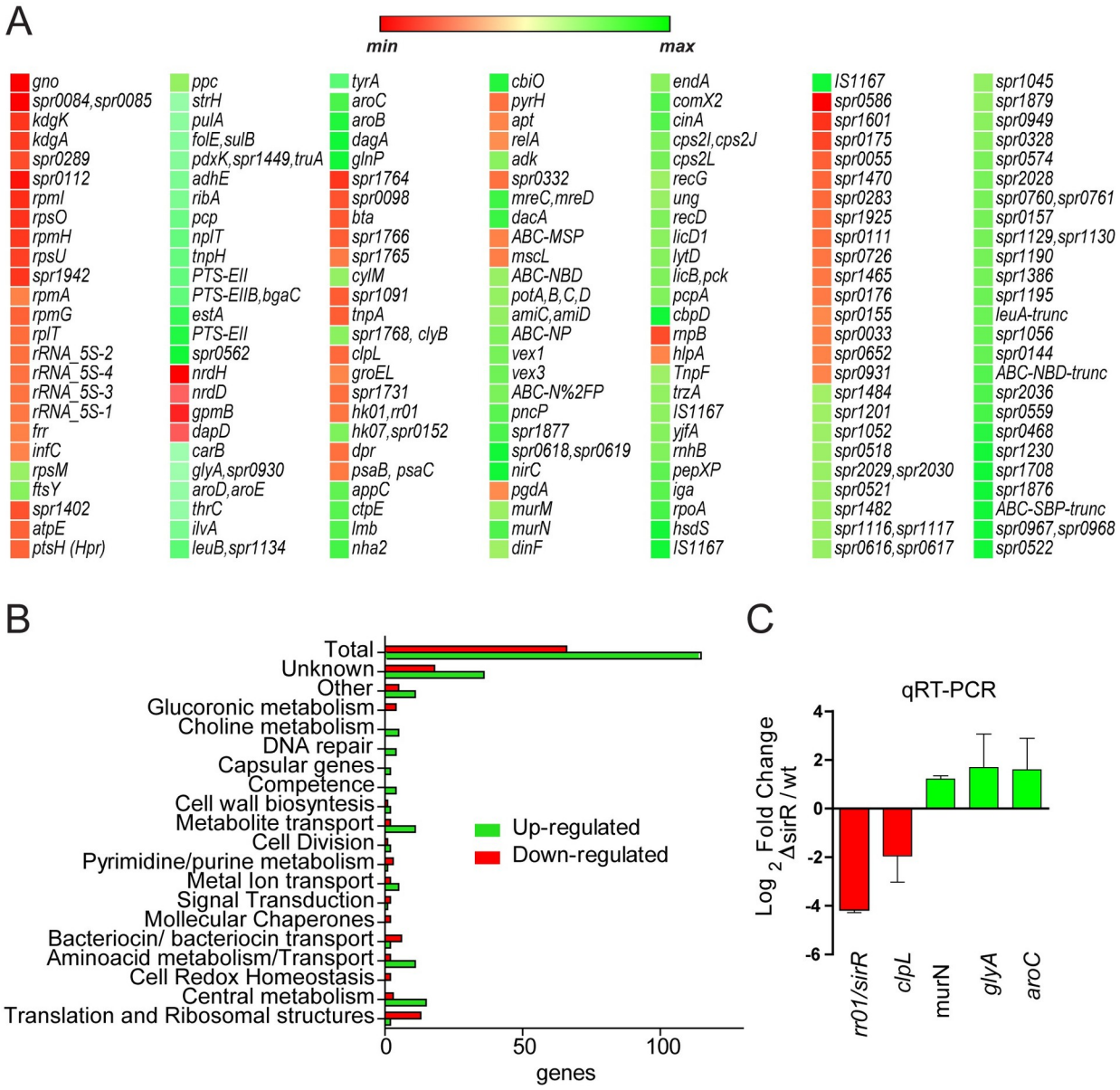

Fig 4. SirR regulates gene expression of the stress response in *S. pneumoniae*. (A) RNA-seq heatmap shows gene expression of the comparison between the Δ*sirR* and *wt* strains incubated in ABM with relative gene expression in $\log_2$ fold change demonstrating increased expression in green and decreased expression in red. Gene expressions higher than 2-fold and *p* values <0.05 were considered significant. (B) Categories of SirR-regulated genes obtained from an RNAseq analysis. An RNAseq generated distribution in functional categories of genes that are regulated in the Δ*sirR* mutant relative to strain *wt*. (C) Putative SirR-regulated genes expressed in the Δ*sirR* mutant relative to strain *wt*. Gene expression determined by RNAseq was confirmed by qPCR. The Δ*sirR* and *wt* strains were grown in BHI to the mid-exponential phase in triplicate and then incubated in ABM for 1h. The fold change in gene expression was measured by RT-qPCR and calculated using the $2^{-\Delta\Delta CT}$ method. The *gyrA* gene was used as internal control.

https://doi.org/10.1371/journal.ppat.1008761.g004

due to the *sirR* deletion itself, we performed a comparative proteomic assay between the *wt* and Δ*sirR* strains under non-stressed conditions (pH 7.0). Of the 925 proteins detected, 21 were downregulated and 41 were upregulated in the Δ*sirR* mutant compared to the *wt* strain (Fig 5A and S4 Table). In addition to ClpL and PsaB, the Δ*sirR* mutant showed reduced expression of Dpr, NrdD, TrxB and GroES regardless of pH. This observation indicates that

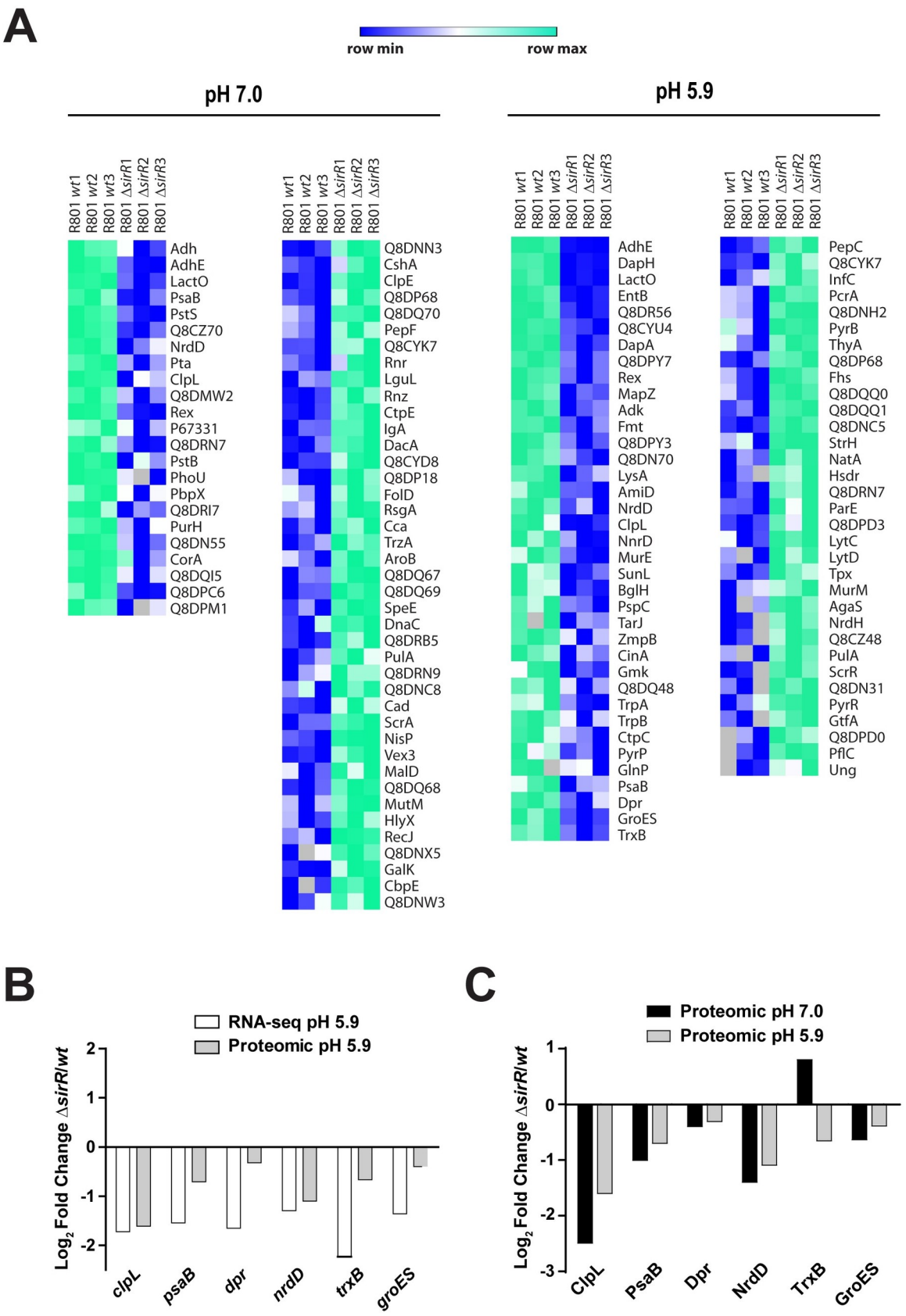
A
row min
row max
pH 7.0
pH 5.9
R801 wt1
R801 wt2
R801 wt3
R801 ΔsirR1
R801 ΔsirR2
R801 ΔsirR3
Adh
AdhE
LactO
PsaB
PstS
Q8CZ70
NrdD
Pta
ClpL
Q8DMW2
Rex
P67331
Q8DRN7
PstB
PhoU
PbpX
Q8DRI7
PurH
Q8DN55
CorA
Q8DQI5
Q8DPC6
Q8DPM1
Q8DNN3
CshA
ClpE
Q8DP68
Q8DQ70
PepF
Q8CYK7
Rnr
LguL
Rnz
CtpE
IgA
DacA
Q8CYD8
Q8DP18
FolD
RsgA
Cca
TrzA
AroB
Q8DQ67
Q8DQ69
SpeE
DnaC
Q8DRB5
PulA
Q8DRN9
Q8DNC8
Cad
ScrA
NisP
Vex3
MalD
Q8DQ68
MutM
HlyX
RecJ
Q8DNX5
GalK
CbpE
Q8DNW3
AdhE
DapH
LactO
EntB
Q8DR56
Q8CYU4
DapA
Q8DPY7
Rex
MapZ
Adk
Fmt
Q8DPY3
Q8DN70
LysA
AmiD
NrdD
ClpL
NnrD
MurE
SunL
BglH
PspC
TarJ
ZmpB
CinA
Gmk
Q8DQ48
TrpA
TrpB
CtpC
PyrP
GlnP
PsaB
Dpr
GroES
TrxB
PepC
Q8CYK7
InfC
PcrA
Q8DNH2
PyrB
ThyA
Q8DP68
Fhs
Q8DQQ0
Q8DQQ1
Q8DNC5
StrH
NatA
Hsdr
Q8DRN7
ParE
Q8DPD3
LytC
LytD
Tpx
MurM
AgaS
NrdH
Q8CZ48
PulA
ScrR
Q8DN31
PyrR
GtfA
Q8DPD0
PflC
Ung
B
RNA-seq pH 5.9
Proteomic pH 5.9
Log2 Fold Change ΔsirR/wt
2
1
0
-1
-2
clpL
psaB
dpr
nrdD
trxB
groES
C
Proteomic pH 7.0
Proteomic pH 5.9
Log2 Fold Change ΔsirR/wt
1
0
-1
-2
-3
ClpL
PsaB
Dpr
NrdD
TrxB
GroES

Fig 5. Comparative proteomic analysis of differentially expressed proteins in the Δ*sirR* and *wt* strains under acidic and non-stressed conditions. (A) Heat map of proteins expressed in the Δ*sirR* mutant and referred to *wt*. Proteins with a fold change greater than 2 (less than -1 or greater than 1 on the x-axis of the graph) and a *p*-value < 0.05 were considered as differentially expressed. Higher expression in the *wt* is displayed in shades of green, and higher expression in the Δ*sirR* mutant (compared to *wt*) is showed in shades of blue. (B) Comparison between $\log_2$ folds change (Δ*sirR*/*wt*) obtained by both RNAseq (white bars) and proteomic (gray bars) analysis. (C) Comparison between $\log_2$ folds change (Δ*sirR*/*wt*) obtained by proteomic analysis at both pH 5.9 (gray bars) and pH 7.0 (black bars).

https://doi.org/10.1371/journal.ppat.1008761.g005

expression of these proteins is directly affected by SirR itself and not simply by changes in pH changes (Fig 5C).

In the *wt* strain, the expression of ClpL and PsaB proteins was increased ~200- and 5-fold increases, respectively, at pH 5.9 compared to pH 7.0 (Fig 6A and 6B).

Although the *sirR* mutation negatively impacted the expression of ClpL and PsaB at pH 7.0, it still retained some capacity to increase their expression in response to acidic conditions (pH 5.9) (Fig 6A and 6B), suggesting additional mechanisms involved in the stress response of *S. pneumoniae*.

ClpL and PsaB are involved in the pneumococcal stress response and the synergistic mechanism between influenza A and *S. pneumoniae*

Since the RNAseq and proteomic data pointed to many stress-related genes under the control of SirRH, we focused our study in two particular stress genes, *clpL and psaB*. The *clpL* gene codes for a chaperone that is known to be induced by heat shock [38, 39]. However, experimental evidence showed ClpL is mainly induced under acidic stress. SDS-PAGE comparison of protein extracts from cells grown in ABM (pH 7.8) or incubated in ABM (pH 5.9) showed increased expression of a 78-kDa band under acidic conditions (S12A Fig). Protein sequencing of this band revealed two peptides of 11 and 14 amino acids with 100% homology with the amino acid sequence of ClpL (S12B Fig). ClpL is predicted to have 701 amino acids and a theoretical molecular weight of 77.6 kDa, in line with our observations in SDS-PAGE (78-kDa).

To analyze the *clpL* transcript levels under acidic conditions, the *wt* cells were exposed at either pH 5.9 or pH 7.8, and total RNA was purified and treated as described [16]. We detected an increase of 70 times in the *clpL* transcript when cells were exposed to pH 5.9 (S12C Fig) indicating that the rise in ClpL expression is linked to adaptive changes at transcriptional levels that are triggered under acidic conditions.

To define the role of ClpL in the pneumococcal stress response, we constructed a Δ*clpL* mutant (S1 Table), which displayed a decrease of 10^4 times in its tolerance to acidified media compared with the *wt* strain (Fig 6C). This mutant presented the same acid sensitivity as the Δ*sirR* mutant, as showed before. With the purpose to determine the effect of oxidative stress, the Δ*clpL* cells were also exposed to H_2O_2, which displayed a reduction in H_2O_2 susceptibility of 200 times compared with *wt*, indicating that this chaperone is not only a heat shock protein [38] but is also involved both in acidic and oxidative stress responses (Fig 6D).

To determine the contribution of ClpL in our cellular infection model, A549 cells were infected with the Δ*clpL* mutant, which displayed that its intracellular survival capacity was similar to *wt*. However, when A549 cells were treated with Bafilomycin A1, or were previously infected with IAV, both conditions that expose pneumococci to the acidic environment of autophagosomes for longer, the Δ*clpL* mutant did not show an increased survival as *wt* did (Fig 6E, S13 Fig). Altogether, these findings indicate that ClpL is involved in the acidic stress response, which is in turn required for increased intracellular survival of *S. pneumoniae* in IAV-infected pneumocytes.

Based in the RNAseq assays, we were also interested in the *psaB* gene that encodes for a Mn^{+2} transporter in *S. pneumoniae*. It was reported that the Δ*psaB* mutant displays

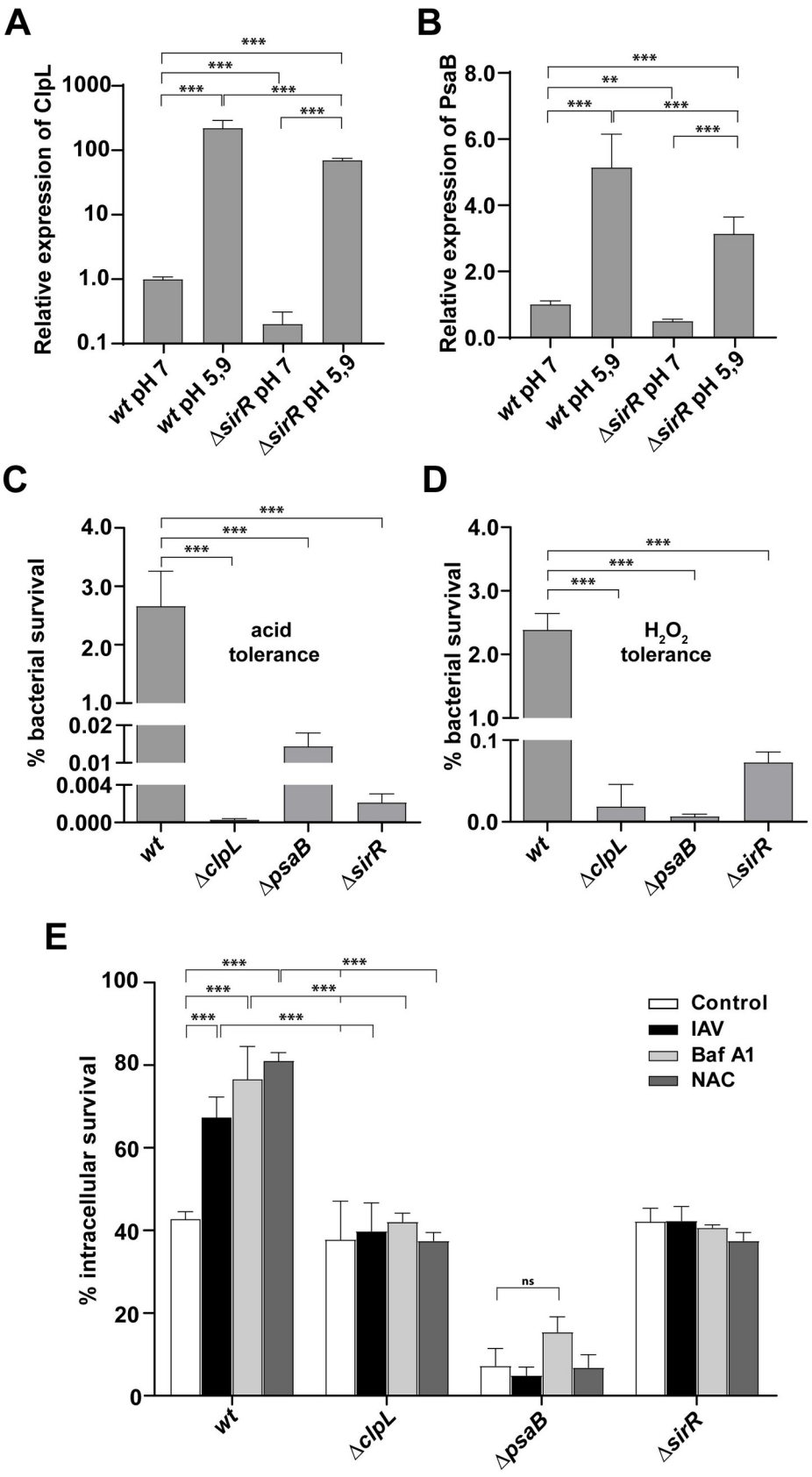
A
Relative expression of ClpL
1000
100
10
1.0
0.1
***
wt pH 7
wt pH 5,9
ΔsirR pH 7
ΔsirR pH 5,9
B
Relative expression of PsaB
8.0
6.0
4.0
2.0
0.0
**
C
% bacterial survival
acid tolerance
0.02
0.01
0.004
0.000
wt
ΔclpL
ΔpsaB
ΔsirR
D
H2O2 tolerance
E
% intracellular survival
ns
Control
IAV
Baf A1
NAC

Fig 6. ClpL and PsaB are involved in the pneumococcal stress response needed for the viral-bacterial synergism. (A) Expression levels of ClpL increased in cells exposed to acidic pH. The *wt* and *ΔsirR* cells were incubated at both pH 7.0 and pH 5.9 for 1h. MS/MS data of ClpL were analyzed and compared. Expression levels of ClpL of different conditions were relativized to ClpL levels of *wt* strain grown at pH 7. (B) Expression levels of PsaB increased in cells exposed to acidic pH. The *wt* and *ΔsirR* cells were incubated at both pH 7 and pH 5.9 for 1h. MS/MS data of PsaB were analyzed and compared. Expression levels of PsaB of different conditions were relativized to PsaB levels of wt strain grown at pH 7. Values represents mean ± SD of three replicates. Data were analyzed using Perseus software [86]. Statistical significance was calculated by Student's t-test, $p<0.01$ (**), $p<0.001$ (***). (C) The Δ*clpL* and Δ*psaB* mutants are susceptible to acidified media. The Δ*clpL*, Δ*psaB*, *ΔsirR* and *wt* cells were grown in BHI until an OD_{620nm} 0.3 and then incubated in ABM medium at pH 4.8 for 1 h. After that, viable cells were assessed as described in the Fig 2 legend. (D) The Δ*clpL* and Δ*psaB* are susceptible to H_2O_2. The Δ*clpL*, Δ*psaB*, Δ*sirR* and *wt* cells were grown in BHI until an OD_{620nm} 0.3 and then exposed at BHI medium containing 20 mM H_2O_2 for 2 h. After that, viable cells were determined as described in the Fig 2 legend. (E) The intracellular survival of *the ΔclpL and psaB mutant* is decreased compared with *wt*. A549 cells were infected with the Δ*clpL*, Δ*psaB* and *wt* cells and intracellular survival was determined as described in the Fig 1 legend. White bars correspond to non-virus infected cells, black bars to IAV-infected cells, light gray bars to Bafilomycin-A1-treated cells and gray bars to NAC-treated cells. For all panels, data are representative of at least three independent experiments and statistically significant differences are indicated as $p<0.01$ (**) or $p<0.001$ (***).

https://doi.org/10.1371/journal.ppat.1008761.g006

susceptibility to oxidative stress [34]. We hypothesized that a lack of *psaB* could influence the intracellular survival of *S. pneumoniae* in IAV-infected cells due to the virus ROS production. The Δ*psaB* mutant strain was 400-fold more sensitive to acidic stress (Fig 6C) and showed 10^4 times more susceptibility to 20 mM H_2O_2 (Fig 6D), in line with previous studies [33, 34]. We also constructed the double Δ*clpL/ΔpsaB* mutant, which displayed an impaired tolerance to oxidative and acidic stress responses, as showed by the individual mutants (S14 Fig).

In contrast to the Δ*clpL* mutant, Δ*psaB* displayed an impaired intracellular survival in non-IAV infected cells (Fig 6E). However, both mutants failed to exhibit increased intracellular survival in IAV-infected or NAC-treated A549 cells, resembling the phenotype observed for the Δ*sirR* mutant (Fig 6E). These observations confirm that ClpL and PsaB are necessary for the IAV-*S. pneumoniae* synergistic mechanism.

In addition to the association with the oxidative stress response, PsaB is mainly part of a Mn^{+2} transporter. To determine the effect of a Mn^{+2} on the bacterial intracellular survival, the *wt* cells were previously incubated in BHI containing 1, 30 or 100 μM of $MnSO_4$ at 37˚C, and these bacterial cells were used to infect A549 cells as described before. We found that this Mn^{+2} pretreatment increased significantly the bacterial intracellular survival, and this phenotype was dependent on the Mn^{+2} concentration (S15 Fig). This finding strengthens the relevance of the regulation of Mn^{+2} transport in the intracellular survival mechanism of *S. pneumoniae*.

Influenza A-*S. pneumoniae* synergism occurs only in autophagy-proficient cells

Previous reports showed that IAV induces autophagy but blocks the last step of the autophagic process [31, 47]. *S. pneumoniae* also induces autophagy [48] and survives in autophagic vesicles [14]. To determine whether autophagy is affected in our IAV-*S. pneumoniae* superinfection model, the potential increased accumulation of LC3-II due to autophagy inhibition was evaluated. As controls of autophagy assays, A549 cells treated with either Bafilomycin A1, a well-known inhibitor of the late phase of autophagy as well [49], or rapamycin, a well-known autophagy inducer [50] showed increased LC3-II levels by Western blot analysis. When A549 cells were infected with either the IAV, the pneumococcal *wt* strain, or superinfected, we detected increased LC3-II levels (S16A and S16B Fig) that are consistent with previous results [51]. In a separate study, mKate2-hLC3 vectors [52] were transfected into A549 cells and subsequently infected by either IAV, *S. pneumoniae* (*wt*, *ΔsirR*, *ΔclpL*, *and ΔpsaB*) or superinfected. Confocal

microscopy results indicated that any of these treatments induced remarkably high mKate2-hLC3 punctations in A549 cells (S17 and S18 Figs). These results together with the increased LC3-II levels in either bacterial or viral infections of A549 cells indicated autophagy induction, as described [14, 48, 51]. During coinfection, we observed that autophagy is also induced in A549 cells, as individual bacterial and viral infections did, and this led us to study in deep the contribution of autophagy in this synergistic mechanism.

To confirm the functional role of autophagy in this viral-bacterial synergism, IAV-infected mouse embryonic fibroblasts (MEF *atg5-KO*), which are deficient in autophagy [53], were superinfected with the pneumococcal *wt* strain. As a control, similar treatments were performed in the parental cell line (MEF *wt*), which are autophagy-proficient cells. A significant increase in the intracellular survival of *S. pneumoniae* in IAV-infected MEF cells was observed similar to that observed in A549 cells (Fig 7A; S19A Fig).

In contrast, S. *pneumoniae* superinfection of IAV-infected MEF *atg5-KO* cells showed a significant decrease in bacterial intracellular survival compared to the bacterial infection only (Fig 7B; S19B Fig). Similarly, the Δ*sirR* mutant showed lower intracellular survival in non-IAV infected MEFs *atg5*-KO relative to non-IAV infected MEFs *wt*, although it was equally deficient in both MEFs *wt* and MEFs *atg5*-KO previously infected with IAV (Fig 7A and 7B; S19 Fig), as observed in IAV-infected A549 cells. Altogether, these results suggest that SirRH mediates the synergistic mechanism between IAV and *S. pneumoniae* and that this phenomenon occurs only in autophagy-proficient cells.

On the other hand, we determined by confocal microscopy that *S. pneumoniae* (blue by DAPI staining) colocalize with an LC3-labeled autophagosome (red by fusion to mKate2) (Fig 7C and 7D). When we quantified these LC3-vesicles containing pneumococci, we observed a significant increase in IAV-infected A549 cells compared with the mock-infected cells (Fig 7E), confirming that IAV infection increases autophagosomes by inhibition of the fusion to lysosomes, as described [14]. We propose that this phenomenon contributes to the intracellular survival mechanism of *S. pneumoniae* in IAV-infected A549 cells.

Discussion

Although *S. pneumoniae* is a common extracellular colonizer of the human nasopharynx, it is known to cause otitis, sinusitis and invasive infections such as pneumonia, bacteremia, and meningitis. Bacterial pneumonia caused by *S. pneumoniae* in patients infected with influenza A has significant relevance in human health during seasonal and pandemic influenza. IAV infections cause physical and physiological changes in the respiratory epithelium that facilitate secondary bacterial infections [10]. Recent reports suggest that such infections are associated with the pneumococcal ability to survive intracellularly. In this regard, Ogawa described intracellular fates of *S. pneumoniae* and found that it is entrapped in specific autophagic vesicles in MEFs [14], which is consistent with our pneumocyte infection model [16]. In the present work, we expanded these studies and found that intracellular pneumococcal survival is clearly improved in IAV-infected pneumocytes.

Many bacterial TCSs, have been involved in intracellular survival mechanisms in eukaryotic cells, such as EvgSA in *Shigella flexneri* [54]; ArcAB [55], PhoPQ [56] and EnvZ/OmpR [57] in *Salmonella* Thyphimurium; SrrAB [58]; GraSR [59] in *Staphylococcus aureus*; PhoPQ in *Escherichia coli* [60]; BvrSR in *Brucella abortus* [61]; and PrrAB in *Mycobacterium tuberculosis* [62], among others. In *S. pneumoniae*, most of the TCSs are required for full virulence in animal models of infection [63, 64] and we have shown that two of these systems, StkP/ComE and CiaRH [15, 16], are important in response to acidic and/or oxidative stress. The poorly studied SirRH system (TCS01) has been previously involved in mediating virulence in intranasally-

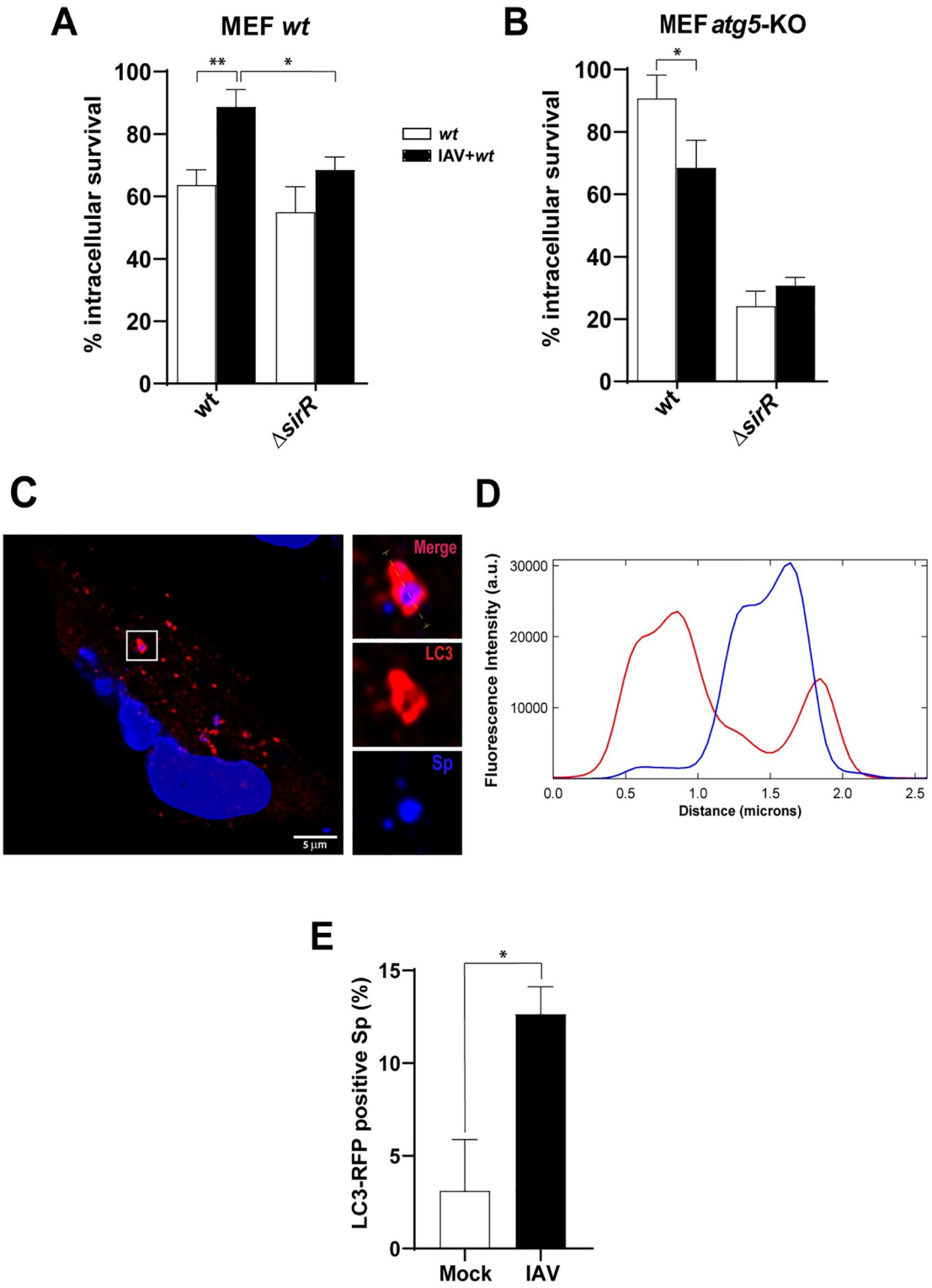

Fig 7. The viral-bacterial synergism is dependent on autophagic-proficient cells. IAV-infected and non-virus MEF (A) and MEF *atg5* KO (B) cells were incubated with the *wt* and the Δ*sirR* strains, and bacterial intracellular survival was assessed as described in the Fig 1A legend. White bars indicate bacterial infection and black bars indicates superinfection. Data are representative of at least three independent experiments and statistically significant differences are indicated as $p<0.05$ (*) or $p<0.01$ (**). (C) IAV-infected A549 cells result in an increased number of *S. pneumoniae*-containing autophagosomes. Representative confocal micrograph showing association of *S. pneumoniae* (dyed with DAPI) with mKate2-hLC3 after 3 hpi, in

A549 cells. IAV-infected and mock-infected A549 cells expressing mKate2-hLC3 were infected with *S. pneumoniae*. The event showed in this panel was localized at z-stack no.11 (out of 29). Scale bar, 5 μm. (D) Multichannel plot profile corresponding to the yellow line in the merge inset in "a" depict the fluorescent intensities (a.u., arbitrary units) of mKate2-hLC3 (red) and DAPI-stained *S. pneumoniae* (blue). (E) Quantification of mKate2-hLC3 association with DAPI-stained *S. pneumoniae* in mock-infected and IAV-infected A549 cells at 3 hpi with *S. pneumoniae*. White bar corresponding to mock-infected cells and black bar to IAV-infected cells. n ≥ 100 bacteria per coverslip. Values represent the mean ± SEM of at least three replicates. Statistical significance was calculated by Student´s t-test (*; $p<0.05$).

https://doi.org/10.1371/journal.ppat.1008761.g007

infected mice [23, 24], and a rabbit endocarditis model [25]; however, the effects on intracellular pneumococcal survival were not explored. Here, we show that the intracellular pneumococcal survival of the Δ*sirR* mutant is similar to the *wt* in A549 pneumocytes, suggesting that this system may not be directly linked to virulence in animal models.

A key finding of our work was that SirR, as well as ClpL and PsaB, are involved in the stress response induced by *S. pneumoniae* and are necessary for the increased pneumococcal survival in IAV-infected cells. ClpL was formerly described as a heat-shock chaperone induced in pneumococcal cells when incubated at 45˚C [39]. The Δ*clpL* mutant is sensitive to temperature (to 43˚C) but virulence remains unaffected in a murine intraperitoneal model [65]. However, ClpL was involved in pathogenicity using a cell model, and it was reported that this chaperone represses the adherence to epithelial cells and induces secretion of TNF-α at the beginning of the invasive process of *S. pneumoniae* [66]. Posteriorly, it was demonstrated that ClpL modulates adherence to pneumocytes mediating activation of the Rap1/Rac1 pathway [67]. On the other hand, ClpL can modulate enzymes responsible for cell wall biosynthesis and decrease penicillin susceptibility [68].

In our hands, we observed that ClpL is mostly induced at pH 5.9 in the *wt* strain. In contrast, the Δ*clpL* mutant does tolerate an acidic pH of ≥4.8 in bacterial culture media. A similar phenotype was reported for *Streptococcus mutans* where ClpL was also induced at pH 5.0 and it was essential for the acid tolerance response [69]. We also found that the Δ*clpL* mutant displayed susceptibility to hydrogen peroxide, indicating that ClpL is likely a chaperone involved not only in thermal but also acidic and oxidative stress responses. Previous reports showed that ClpL's activity is Mn^{+2}-dependent [70], further adding to its potential relevance of these proteins in the general stress response of *S. pneumoniae*. Our studies suggest that that ClpL is a key chaperone related to the general stress response of *S. pneumoniae* and essential for bacterial intracellular survival in IAV-infected cells.

PsaB was previously described as an ATP-binding protein that belongs to the ABC-type manganese permease [71]. Mutations on the genes that constitute the *psaBCA* operon result in growth limitations in culture media with low Mn^{+2} concentration, and attenuation in four different animal models of infection [72]. The PsaBCA complex is indeed a Mn^{+2} transporter and its protein components are involved in virulence, resistance to hydrogen peroxide and superoxides [34]. The *psaBC* mutant shows hypersusceptibility to hydrogen peroxide and superoxides [73]. We observed the same phenotype in our Δ*psaB* mutant, confirming that this strain is more susceptible to exogenous hydrogen peroxide than the *wt* strain. Since the *S. pneumoniae* Δ*sirR*, Δ*clpL* and Δ*psaB* mutants showed alterations to both acidic and oxidative stress conditions, it suggests a common strategy to general stress adaptation that involves, at least, a TCS, a chaperone and a Mn^{+2} transporter. Such cross-response mechanisms are not unique to *S. pneumoniae*. In *Streptococcus mutans*, a cross-response effect between acidic and oxidative stress was reported for a mutant of the oxidative stress regulator SpxA. Similar to the *S. pneumoniae* Δ*sirR* mutant, the *spxA* mutation impairs *S. mutans'* ability to grow under acidic and oxidative conditions [74].

We observed that SirR controls transcription of the *clpL* and *psaB* genes by unknown mechanisms. The SirR response regulator modulates the acidic/oxidative stress response of *S. pneumoniae* to improve intracellular survival in influenza-infected cells. However, transcription of the *clpL* and *psaB* genes could be co-regulated by other regulators [70]. For example, the conserved repressor CtsR regulates the *clpL* expression in many streptococci and lactococci, and these bacteria present CtsR box elements in the *clpL* promoter region [70]. In *S. pneumoniae*, CtsR-binding sites were located upstream from the *clpL* gene [75], however, its regulation has not been yet elucidated. Based on the qPCR assays, we suggest that the *clpL* expression is induced by acidic pH and controlled by SirR, but we cannot discard the possibility that other regulators such as CtsR modulate ClpL stress response in *S. pneumoniae*. Equally complex appears to be the regulation of the *psaB* gene. The expression of the *psaBCA* operon is controlled by the PsaR regulator in a Mn^{+2}-dependent manner [76]. In addition, RR04, which belongs to the TCS04, is necessary for the activation of the *psaBCA* locus [32]. Here, we demonstrate that SirR is also essential for the transcriptional activation of the *psaB* gene, adding to complexity of this regulation. Regarding the increased intracellular survival of *S. pneumoniae* in IAV-infected A549 cells, it is clear that SirR is necessary for IAV-infected cells but for not in non-infected cells.

Without a previous IAV infection, there is a subpopulation of pneumococci that can survive intracellularly under acidic conditions in autophagosomes, however, another subpopulation dies because it is not adapted to this stress condition, or it is degraded by fusion to lysosomes. Under these stress conditions, the *wt* strain does not need the stress response controlled by the SirH two-component system that regulates the expression of many genes, such as *clpL* and *psaB* among others. For these reasons, we think that the Δ*sirR*, Δ*sirH*, and Δ*clpL* mutants did not show an impaired intracellular survival compared with the *wt* strain.

IAV infection likely produces stress conditions in pneumocytes that *S. pneumoniae* overcomes in a SirRH-dependent manner to improve its capacity to survive intracellularly. Based on the bacterial survival assay in acidified media, where the Δ*sirR*, Δ*clpL*, and Δ*psaB* cells showed impaired acidic tolerance, we suggest that *S. pneumoniae* needs an adaptive process to survive under acidic conditions, such in acidic vesicles in IAV-infected pneumocytes.

During infection, the viral M2 proton pump of IAV blocks the autophagosome/lysosome fusion [31]. Thus, in IAV-infected cells, *S. pneumoniae* is faced with more prolonged exposure in acidic vesicles and increased ROS compared to non-virus infected cells, promoting a stress response that is mediated by the SirRH TCS. Coincidentally, the Δ*sirR*, Δ*sirH*, Δ*clpL*, *and* Δ*psaB* mutants show impaired survival in IAV-infected cells; however, except for the Δ*psaB* mutant, their intracellular survival is similar to the *wt* strain in non-virus infected cells. These observations are in line with the results obtained from bacterial survival assays in both acidified and H_2O_2-containing media and in the studies in which A549 cells were treated with either Bafilomycin A1 or NAC.

Taking into account that ClpL expression is induced at pH 5.9 in the *wt* strain and that the Δ*sirR* cells show decreased ClpL and PsaB expression, we do not have experimental evidence that this TCS senses directly pH, but SirRH is likely sensing environmental conditions involved in the acidic stress response that this pathogen uses to modulate adaptation to such condition (Fig 8).

Related to the putative role of oxidative stress in the synergistic mechanism between IAV and *S. pneumoniae*, it is known that IAV infection increases ROS production in A549 cells [77]. It was reported that *S. pneumoniae* induces an oxidative stress response to survive under oxidative conditions [78]. Analyzing the list of SirR-regulated genes, we focused our attention on the *psaB* gene that encodes for a Mn^{+2} transporter involved in oxidative stress response in *S. pneumoniae* [34, 79]. It was described that the Δ*psaB* mutant was very sensitive to hydrogen

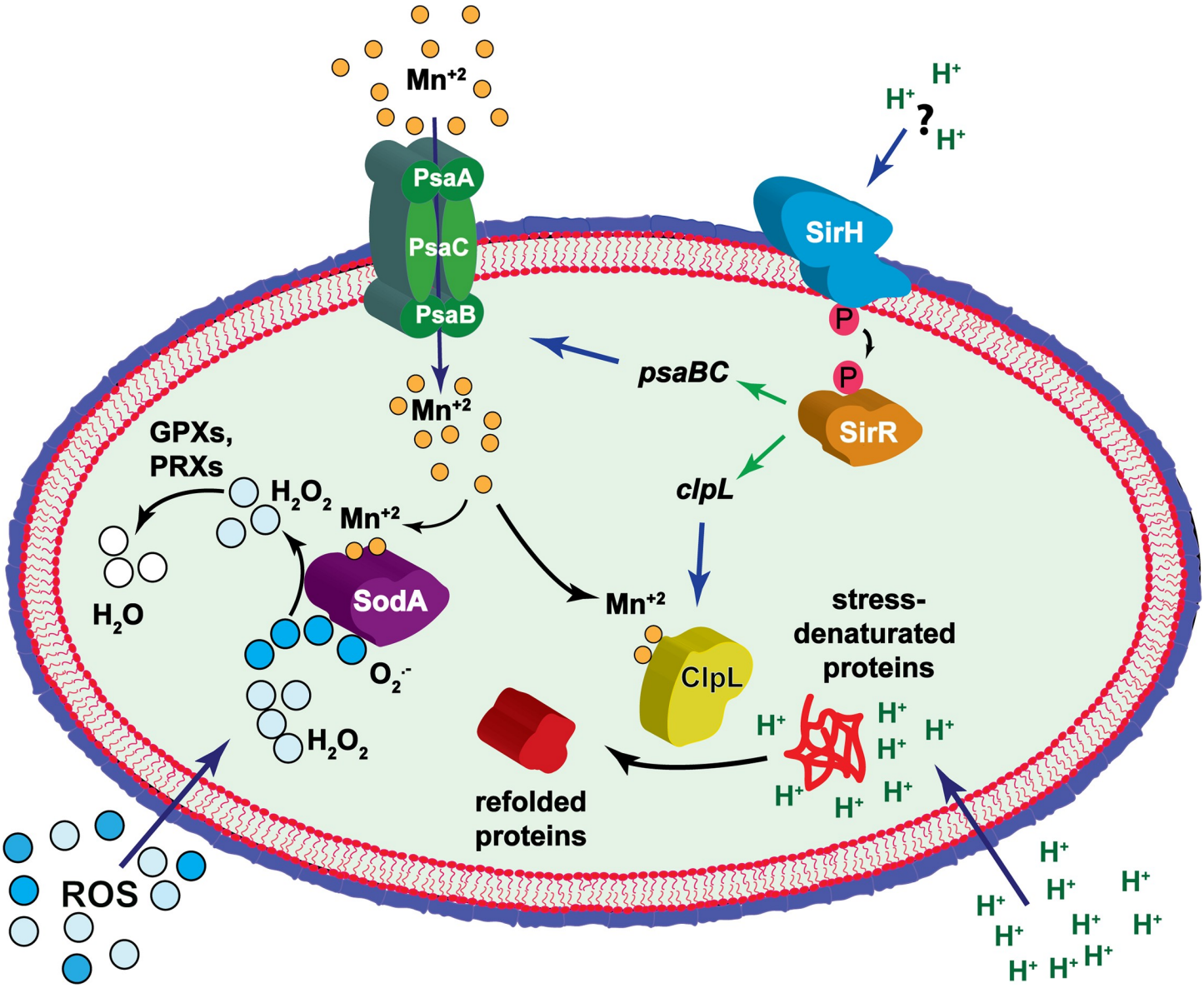

Fig 8. Proposed model for the synergistic mechanism that exists between influenza A and *S. pneumoniae* in pneumocytes.

https://doi.org/10.1371/journal.ppat.1008761.g008

peroxide, and this probably occurs due to a low Mn^{+2} level that affects the SodA activity [79]. In view of our results, SirR controls, directly or indirectly, *psaB* transcription affecting the oxidative stress tolerance supported by SodA. To confirm this hypothesis, we tested the Δ*sodA* mutant and we found the same phenotype that the Δ*sirR* and Δ*psaB* mutants, which showed increased susceptibility to hydrogen peroxide. Curiously, the Δ*clpL* mutant also displayed an impaired hydrogen peroxide tolerance, suggesting that ClpL is essential for general stress response. Regarding a putative cross stress response, it is important to highlight that ClpL is a Mn^{+2}-dependent chaperone [38], in consequence, there is a direct association with the PsaB Mn^{+2} transporter. Probably, in the Δ*psaB* mutant, the observed decreased tolerance to acidic pH that corresponds to diminished activity of ClpL is also due to a low Mn^{+2} level.

The importance of oxidative stress response in the intracellular survival mechanism of *S. pneumoniae* was revealed when ROS production was inhibited in A549 cells by a NAC treatment during bacterial infection. Under these conditions, we observed that the *wt* strain increased its survival, as described for A549 cells [48], indicating that *S. pneumoniae* must overcome this type of stress to survive intracellularly and that this pathogen is susceptible to changes in ROS levels. In the intracellular context of IAV-infected pneumocytes, this virus can increase ROS production [36] and, to achieve synergism, *S. pneumoniae* should be also able to overcome oxidative stress.

Our results indicate that the lack of PsaB impaired the intracellular survival of *S. pneumoniae*, even in non-IAV infected cells, probably because Mn^{+2} is needed in for many bacterial processes [80]. In contrast, SirR and ClpL were not essential for this survival mechanism but SirR, ClpL, and PsaB were found to be necessary for the synergism detected in *S. pneumoniae* in IAV-infected A549 cells. We propose that *S. pneumoniae* needs to induce a SirR-controlled adaptive process during superinfection to express chaperones, such as ClpL, to refold proteins denatured by acidic stress and by the IAV-induced ROS production [36], and Mn^{+2} transporter to provide this metal that is essential for chaperone activity, among other cellular processes (Fig 8).

As mentioned before, Gannage *et al* [31] reported that IAV infection produced an accumulation of autophagosome by IAV M2-induced blockage of fusion with lysosomes. On the other hand, Ogawa *et al*. [14] reported that *S. pneumoniae* is able to survive in autophagic vesicles. Based on these findings, we hypothesized that the IAV-*S. pneumoniae* synergism may depend on the autophagic process. This putative autophagy-dependence was confirmed using the MEF cell line, with which we reproduced the same synergism found in A549 cells, but not in the MEF *atg5*-KO cells that are deficient in autophagy, indicating that this synergistic mechanism occurs only in autophagy proficient cells. Furthermore, fewer pneumococci colocalizing with acidic vesicles, but more pneumococci associated with LC3-positive vesicles in IAV-infected cells, support the notion that inhibition of autophagosome-lysosome fusion step during IAV infection favors increased pneumococcal intracellular survival.

Pneumococcal pathogenesis has been studied extensively in the last decades. Although *S. pneumoniae* is considered a typical extracellular pathogen, particular attention has been given to the intracellular survival mechanism in the last years, as mentioned before [13–16]. In this work, we report for the first time that the intracellular survival of *S. pneumoniae* is enhanced in IAV-infected cells, and this synergism occurs in autophagic-proficient cells. For this survival, *S. pneumoniae* needs a physiological adaptation to IAV-induced conditions, and we propose that the SirRH TCS probably senses these changes at intracellular level and controls the expression of ClpL and PsaB, which are needed to tolerate the acidic pH found in intracellular vesicles, as well as the increased ROS level produced by influenza A.

We consider that our results contribute to the knowledge of the intracellular survival mechanism of *S. pneumoniae* in the context of pulmonary cells infected with influenza A, with a consequent relevance for the management of secondary infections in influenza-infected patients. We propose that intracellular antibiotics should be also considered for the treatment of pneumococcal infections during an epidemic or pandemic influenza A. Many works have described this particular viral-bacterial synergism [1, 8–11], and here we provide experimental evidence on how influenza A infections enhance the intracellular survival of *S. pneumoniae*.

Materials and methods

Ethics statement

Embryonated chicken eggs were harvested in accordance with standardized protocols described in the WHO Manual on Animal Influenza Diagnosis and Surveillance [83]. No animal experiments were performed.

Bacterial and viral strains, plasmids, cell lines, and growth conditions

All bacterial strains, oligonucleotides and plasmids used in this study, as well as cloning and mutagenesis procedures, are listed in the supplementary material (S1 Table). Oligonucleotide synthesis and DNA sequencing service were performed in Macrogen Inc. (Seoul, South Korea). The growth conditions and stock preparation for the pneumococcal and *Escherichia coli* strains have been reported elsewhere [28], and the transformation assays have been previously described [81].

IAV cultivation in embryonated chicken eggs

The influenza virus A/Puerto Rico/8/1934 (H1N1) (IAV) strain was used for superinfection assays. Specific pathogen-free embryonated chicken eggs were obtained from Avico (Argentina). Viruses were grown in 11-days-old embryonated chicken eggs, which were incubated for 72 h at 37˚C The allantoic fluid was collected, aliquoted, titrated in Madin-Darby canine kidney cells (MDCK; ATCC CCL-34) (50% tissue culture infective doses [$TCID_{50}$]) and eggs (50% egg infective dose [EID_{50}]), and stored at −80˚C until used [82].

Cell lines and culture conditions

The A549 cell line (human lung epithelial carcinoma, pneumocytes type II; ATCC CCL-185™) and the HeLa cell line (human cervix epithelial adenocarcinoma; ATCC CCL-2) were cultured at 37˚C, 5% CO_2 in Dulbecco's modified Eagle medium (DMEM) with 4.5 g/l of glucose and 10% of heat-inactivated fetal bovine serum (FBS) (Gibco BRL, Gaithersburg, Md.). Fully confluent A549 cells were split once every two or three days via trypsin/EDTA treatment and diluted in fresh media before being cultivated in Filter cap cell flasks of 75 cm^2 (Greiner Bio-one no. 658175) until passage 6, as described [16]. A549 cells were transfected/co-transfected with pIRES2-EGFP and pIRES2-M2 using JetPRIME (Polyplus-transfection, Illkirch, France) following the manufacturer's instructions in serum-free DMEM (Invitrogen) supplemented with 5% of Fetal Bovine Serum (FBS). The MEF (Mouse Embryonic Fibroblast) and the autophagy-deficient MEF *atg5-KO* cell lines were generously provided by Dr. Noboru Mizushima [53]. These cell lines were cultured under the same conditions as described for A549 and HeLa cells. The mKate2-LC3 plasmids [52] were obtained from Addgene. The 16HBE14o- cell line (human bronchial cells immortalized with the origin-of-replication defective SV40 plasmid) [22] was originated by Dr. Dieter Gruenert (University of California-San Francisco, USA), and it was kindly provided by Dr. Beate Illek (University of California-San Francisco, USA). The 16HBE14o- cells were cultured as described [84].

Intracellular survival assays

The intracellular survival assays of pneumococci were performed as reported previously [15, 16] with modifications. Briefly, approximately 1.5×10^5 of eukaryotic cells (A549, 16HBE14o-, MEF, MEF *atg5-KO*, HeLa cell lines) per well were seeded in 12-well plates and cultured in DMEM + 5% FBS and incubated at 37˚C and 5% CO_2 for 24 h, until to 90–95% confluence that corresponds approximately to 3.0 x 10^5 cells. On the other hand, pneumococci were grown in BHI to the mid-log phase (OD_{600nm} 0.3) and resuspended in DMEM (with 5% FBS). The infection of cell monolayers was carried out using a multiplicity of infection (MOI) 30:1 (9 x 10^6 bacteria: 3 x 10^5 cells). For the rest of the cell lines (16HBE14o-, MEF, MEF *atg5* KO and HeLa cells), we used the same procedure of pneumococcal infection of A549 cells. For bacterial internalization, A549 cells were incubated 3 h with pneumococci at 37˚C and 5% CO_2. To eliminate pneumococci that were not internalized into A549 cells, supernatants were discarded, and fresh DMEM (with 5% FBS) containing the extracellular antibiotic gentamicin sulfate (150 μg/ml; US Biological G2030) was added to the infected cells. After a 30 min period of

antibiotic treatment at 37˚C, cells were washed three times with PBS. The bacterial survival obtained just after the antibiotic treatment corresponds at time zero (t = 0). To determine a time curve for bacterial survival, the bacterial-infected A549 cells were cultured in DMEM + 5% FBS and incubated at 37˚C and 5% CO_2 for 2 hs more after the antibiotic treatment. As a control, the A549 cells were trypsinized and the occurrence of apoptosis/necrosis caused by pneumococcal infection was quantified by flow cytometry (Annexin V/propidium iodide labeling kit; Invitrogen) giving 5% approximately for all time points analyzed.

To determine intracellular bacterial survival, cells were lysed by centrifugation for 5 min at 10,000 *g* and the bacterial pellet was resuspended in THYE medium. The number of internalized bacteria was quantified after serial dilutions of lysates and plating on BHI 5% sheep blood agar plates with incubation for 16 h at 37˚C. The number of surviving bacteria obtained a t = 0 was defined as a 100% survival, and the data obtained at 2 h were referred to t = 0 to calculate the respective percentages. The reference data (100%) at t = 0 was not included in figures.

For intracellular survival determinations in the viral-bacterial superinfection assays, approximately 1.5×10^5 of eukaryotic cells (A549, MEF *wt*, MEF *atg5-KO*, HeLa and 16HBE14o- cell lines) per well were seeded in 12-well plates to a 90–95% confluence, cultured in DMEM + 5% FBS and incubated for 24 h. Posteriorly, DMEM + 5% FBS was removed from plates, cells were washed three times with PBS and cultured with DMEM containing 1 μg/mL TPCK-treated trypsin for 1 h. Then, approximately 3 x 10^5 cells were infected with IAV at a viral MOI of 10 at 37˚C for 24 h. In parallel, the occurrence of apoptosis/necrosis produced by IAV infection was determined by flow cytometry (Annexin V/propidium iodide labeling kit; Invitrogen) and it was approximately 5%.

To perform bacterial survival assays in IAV-infected cells, we carried out the same protocol of bacterial infection described above. A549 cells were treated with either 100 nM Bafilomycin A1 or with 5mM NAC at the same time that bacterial infection (3 h). These agents were removed when cells were washed with PBS before antibiotic treatment to kill extracellular bacteria. To test probable effects of Bafilomycin A1 or NAC on the normal growth of pneumococcal strains, bacterial cells were incubated in the DMEM+FBS 5% containing 100 nM of Bafilomycin or 5 mM NAC for 3 h at 37˚C, and bacterial growth was determined by turbidity of bacterial cultures by measuring the absorbance value at OD_{600nm}.

Susceptibility to acidic and oxidative stress

To determine susceptibility to acidic pH, bacterial cells were grown in Brain Heart Infusion (BHI; pH 7.2) at 37˚C until OD_{600nm} ~ 0.3, centrifuged at 10,000 *g* for 5 min, resuspended in Todd Hewitt-Yeast Extract (THYE; pH 4.8) and incubated for 1 h at 37˚C. To measure susceptibility to oxidative stress, bacterial cells were grown in BHI at 37˚C until OD_{600nm} ~ 0.3, and 20 mM H_2O_2 was added to the cultures for 1 h at 37˚C. To determine the survival percentage in these assays (acidic and oxidative conditions), serial dilutions were made in THYE (pH 7.8) and plated onto 5% of sheep blood tryptic-soy agar (TSA) plates. After 24 h of incubation at 37˚C, colonies were counted to determine the number of survivors. The percentages were calculated by dividing the number of survivors, at pH 4.8 or 20 mM H_2O_2, by the number of total cells at time zero before incubation at stressful conditions. Data were expressed as the mean percentage ± standard deviation (SD) of independent experiments performed in triplicate.

In-gel tryptic digestion and amino acid sequencing of protein bands separated by SDS-PAGE

The protein band of 78 kDa, separated by SDS-PAGE and stained by Coomassie Blue, was cut and the gel slice was incubated in 100 mM ammonium bicarbonate (pH 8.3) containing 45

mM dithiothreitol at 60˚C for 30 min. The sample was cooled at RT, and 100 mM iodoacetamide was added followed by incubation at RT in the dark for 30 min. The gel was then washed in 50% acetonitrile-100 mM ammonium bicarbonate with shaking for 1 h, cut in pieces, and transferred to a small plastic tube. Acetonitrile was added to shrink the gel slices and dried in a rotatory evaporator. Then, the gel pieces were treated with 100 mM ammonium bicarbonate (pH 8.3) containing trypsin at a 10:1 ratio (w/w, substrate: enzyme). The sample was incubated at 37˚C for 16 h, and digestion products were extracted twice from the gel with 0.1% trifluoroacetic acid for 20 min. Extractions were loaded into a C18 high-pressure liquid chromatography column (220 × 1 mm), and peptides were eluted with 80% acetonitrile-0.08% trifluoroacetic acid. Selected peaks were applied to a 477A protein-peptide sequencer equipped with a 140 HPLC (Applied Biosystems) and subjected to Edman degradation sequence analysis at the Laboratorio Nacional de Investigacion y Servicios en Péptidos y Proteinas facility (CONICET) [85].

Mass Spectrometry Analysis

Protein digestion and Mass Spectrometry analysis were performed at the Proteomics Core Facility CEQUIBIEM, at the University of Buenos Aires/ CONICET (National Research Council) as follows. Protein samples were reduced with dithiothreitol (DTT) in 50 mM of ammonium bicarbonate at a final concentration of 10 mM (45 min, 56˚C) and alkylated with iodoacetamide in the same solvent at a final concentration of 30 mM (40 min, RT, in darkness). Proteins were digested with trypsin (Promega V5111). After that, the peptides were purified and desalted with ZipTip C18 columns (Millipore). The digests were analyzed by nano-LC-MS/MS in a Q-Exactive Mass Spectrometer (Thermo Scientific) coupled to a nano-HPLC EASY-nLC 1000 (Thermo Scientific). For the LC-MS/MS analysis, approximately 1 μg of peptides were loaded onto the column and eluted for 120 minutes using a reverse-phase column (C18, 2 μm, 100A, 50 μm x 150 mm) Easy-Spray Column PepMap RSLC (P/N ES801) suitable for separating protein complexes with a high degree of resolution. The flow rate used for the nano-column was 300 nL min-1 and the solvent range from 7% B (5 min) to 35% (120 min). Solvent A was 0.1% formic acid in water whereas B was 0.1% formic acid in acetonitrile. The injection volume was 2 μL. The MS equipment has a high collision dissociation cell (HCD) for fragmentation and a Q-Exactive Orbitrap analyzer (Thermo Scientific). A voltage of 3.5 kV was used for Electro Spray Ionization (Easy-Spray; Thermo Scientific,). XCalibur 3.0.63 (Thermo Scientific) software was used for data acquisition and equipment configuration that allows peptide identification at the same time of their chromatographic separation. Full-scan mass spectra were acquired in the Orbitrap analyzer. The scanned mass range was 400–1800 m/z, at a resolution of 70000 at 400 m/z and the twelve most intense ions in each cycle were sequentially isolated, fragmented by HCD and measured in the Orbitrap analyzer. Peptides with a charge of +1 or with unassigned charge state were excluded from fragmentation for MS2.

Analysis of MS data

Q-Exactive raw data was processed using Proteome Discoverer software (version 2.1.1.21 Thermo Scientific) and searched against *Streptococcus pneumoniae* (strain ATCC BAA-255 R6) UP000000586 protein sequences database with trypsin specificity and a maximum of one missed cleavage per peptide. Proteome Discoverer searches were performed with a precursor mass tolerance of 10 ppm and a product ion tolerance to 0.05 Da. Static modifications were set to carbamidomethylation of Cys, and dynamic modifications were set to oxidation of Met and N-terminal acetylation. Protein hits were filtered for high confidence peptide matches with a

maximum protein and peptide false discovery rate of 1% calculated by employing a reverse database strategy.

Proteome Discoverer calculates an area for each protein in each condition. To do this it uses the area under the curve of the 3 most intense peptides for a protein. Areas were calculated for each of the three triplicates and normalized. The data obtained for the area for each protein were processed with the Perseus program (Max Planck Institute of Biochemistry, 1.5.5.3 version, available for free) [86] that allows a deeper statistical analysis. Different scatter plots were done according to the compared samples. For each couple of samples, we plotted log *p*-value (-log Student T-test *p*-value A_B) on the y-axis versus Student T-test Difference A_B in the x-axis. Proteins that appear in the volcano plot with a fold change greater than 2 (less than -1 or greater than 1 on the x-axis of the graph) and a p-value < 0.05 (above 1.3 on the y-axis of the graph) were considered as differentially expressed.

RNAseq analysis

Cells were initially grown in THYE medium at pH 7.8 until OD_{600nm} ~0.3 (log phase), centrifuged at 14,000 g for 10 min at 4˚C, resuspended in the same volume in ABM at pH 5.9 [28] and incubated a 37˚C for 1h. Then, cells were centrifuged at 14,000 x g for 10 min at 4˚C, resuspended in a 1/10 vol of lysis buffer (DOC 1% in 0.9% Na Cl) and incubated 3 min a 37˚C until complete lysis. Total RNA from three biological replicates for *wt* and the Δ*sirR* mutant were purified by TRIzol reagent according to the manufacturer's instructions (Fisher Scientific). The RNA for RNAseq assays was obtained as described [16]. Data analysis was performed as reported [70].

Differential gene expression

The aligned reads were assembled by Cufflinks (version-2.2.1), and then the differentially expressed genes were detected and quantified by Cuffdiff, which is included in the Cufflinks package, using a rigorous sophisticated statistical analysis. The expression of the genes was calculated in terms of FPKM (fragment per kilobase per million mapped reads). Differential gene expression analysis was carried out between *wt* and the Δ*sirR* samples.

Protein analysis by western blots

The A549 cells were lysed and protease inhibitor cocktail added to obtain the whole protein to be quantified. The lysates with protein loading buffer were boiled for 5 min. The supernatants were collected and 40 μg of each sample were loaded onto 15% SDS-PAGE gels and electrophoresed for protein resolution at RT using Tris-Glycine-SDS running buffer at a constant electric field of 100 V cm-1. Posteriorly, proteins were electroblotted onto PVDF membranes, which were blocked for 2 h at room temperature and incubated overnight at 4˚C with primary antibodies diluted at 1:1,000 in PBS with 5% bovine serum albumin buffer. After washing 3 times with Tris-buffered saline (TBS) with 0.5% (v/v) Tween, the membranes were incubated for 2 h at room temperature with Alexa-conjugated secondary antibody (1:1,000 dilution) to detect LC3-II and p62. The membranes were imaged under fluorescence mode in an Oddisey CLx Imaging System (LI-COR), and bands were quantified with Image Studio software (LI-COR). Rabbit monoclonal antibody against LC3A/B (D3U4C) XP (12741P) was obtained from Cell Signaling Technology. Rapamycin (R8781; Rapa, mTOR inhibitor), Bafilomycin A 1 from *Streptomyces* (B1793) and Mouse monoclonal anti-beta-actin antibody (A2228) were obtained from Sigma Life Science. Mouse monoclonal antibody against Influenza A M2 protein [14C2] (ab5416) was obtained from Abcam. Recombinant Rabbit monoclonal antibody against SQSTM1/p62 (701510) was purchased to Invitrogen.

qRT-PCR

cDNA was synthesized from 2 μg RNA using the ProtoScript II First Strand cDNA Synthesis Kit (NEB) following the manufacturer's protocol, and cDNA was cleaned using the QIAquick PCR Purification Kit (Qiagen). Genes were amplified using the oligonucleotides listed in the S5 Table and PowerUp SYBR Green Master Mix (Applied Biosystem) following the manufacturer's protocol. Expression was determined relative to AU0158 normalized by *gyrA* (*spr1099*) expression using the ΔΔCt method [87]. The *gyrA* had a similar expression by RNA-Seq for *wt* and the Δ*sirR* mutant, and this had been used to normalize the expression in *S. pneumoniae* in other studies [88].

ROS detection

To assess ROS production, we used 2′,7′-Dichlorodihydrofluorescein diacetate dye (H_2DCF-DA; Molecular Probes) following the manufacturer's instructions. Briefly, we infected A549 cells with IAV at MOI 10 as it was indicated above, 24 h post-infection the cells were trypsinized and washed twice with PBS, resuspended with PBS containing H_2DCF-DA (10 μM) and incubated for 30 min at 37˚C. Then, cells were washed and resuspended with PBS and we measured the intensity of fluorescence of the DCF by cytometry.

Fluorescence Imaging

For the determination of association of *S. pneumoniae*-containing vesicles with LysoTracker Deep Red by immunofluorescence detection, A549 cells were seeded at 1,5 x 10^5 cells per well on glass coverslips in 12-well plates. The infection with IAV and *S. pneumoniae* was performed as described above. Cells were incubated with 1 μM LysoTracker Deep Red (Invitrogen, USA) for 30 min before fixation to stain lysosomes. To analyze the expression of LC3-II in A549 cells infected by IAV, S. pneumoniae, or superinfected, as well as the association between *S. pneumoniae* and LC3, A549 cells were previously transfected with LC3-mKate2 plasmid using Jet-PRIME (Polyplus-transfection, Illkirch, France), and 24 h later were infected as described before. In both cases, at 3 hpi with *S. pneumoniae*, cells were washed 3 times with PBS, fixed with 2% paraformaldehyde– 2% sucrose for 15 min followed by DAPI staining. Finally, coverslips were washed with PBS and mounted on glass slides using Mowiol 4–88. Images were acquired using confocal microscopes (Zeiss LSM-800 and Olympus FV-1200) under 63X oil objectives. Images were processed with ImageJ 1.51n.

Accession numbers

The RNA-Seq data generated from this study are deposited at the NCBI SRA under the accession numbers SAMN08473835 (*wt* strain) and SAMN08473837 (Δ*sirR* strain). This data corresponds to the Bioproject PRJNA433281, and the SRA IDs are SRR6679010 and SRR6679012.

Supporting information

S1 Fig. Determination of apoptosis and necrosis levels in A549 cells infected with IAV and/or S. *pneumoniae*. (A) A549 cells were infected with different MOI of IAV for 24 h and coinfected with a bacterial MOI of 30. Apoptosis/necrosis was measured at the single-cell level by labeling cells with annexin-V-APC and counterstaining with propidium iodide (PI). Representative data are shown and percentage of cells are indicated in each quadrant (lower left: APC^-/PI^-, intact cells; lower right: APC^+/PI, apoptotic cells; upper left: APC^-/PI^+, necrotic cells; upper right: APC^+/PI^+, late apoptotic or necrotic cells). (B) The bar chart describes the percentage distribution of necrotic, apoptotic and viable cells after infection with different

MOI of IAV or with superinfection with *S. pneumoniae*. (C) A549 cells were superinfected with a viral MOI of 10 using either heat-inactivated (at 56˚C for 30 min) or active virus particles, and the percentage of intracellular bacterial survival was performed as described in Fig 1.
(TIF)

S2 Fig. Enhancement of pneumococcal intracellular survival by Influenza A infection is mediated by the SirRH two-component system. Raw data corresponding to the superinfection assays shown in Fig 1A, and for the superinfection assays in A549 cells using the pneumococcal *wt*, Δ*sirR*, Δ*sirR*, *hk01*::pJDC9 and *wr sirR*+ strains in Fig 1B. (A) We represented CFU counting per well at time 0h and 2h corresponding to the superinfection assays of A549, HeLa, MEF and 16HBE14o- cells shown in Fig 1A. White bars correspond to CFU at 0h and grey bars to CFU to 2h. Values represent mean ± SD. In the upper-table are represented the values of all replicates of each sample. In the bottom-table are represented the percentages of survival of all replicates of each sample. (B) We represented CFU counting per well at time 0h and 2h corresponding to the superinfection assays in A549 cells using the pneumococcal *wt*, Δ*sirR*, Δ*sirR*, *hk01*::pJDC9 and *wr sirR*+ strains shown in Fig 1B. White bars correspond to CFU at 0h and grey bars to CFU to 2h. Values represent mean ± SD. In the upper-table are represented the values of all replicates of each sample. In the bottom-table are represented the percentages of survival of all replicates of each sample.
(TIF)

S3 Fig. Analysis of the intracellular survival of R801, R6 and D39 strains in IAV-infected A549 cells. (A) A549 cells were superinfected with IAV and the pneumococcal R801, R6 and D39 *cpsB* strains. White bars correspond to pneumococci-infected cells and black bars to superinfected cells. (B) The raw data presented in this panel correspond to the assays shown in panel A. We represented CFU counting per well at time 0 h and 2 h, white bars correspond to CFU at 0h and grey bars to CFU to 2h. Values represent mean ± SD. In the upper-table are represented the values of all replicates of each sample. In the bottom-table are represented the percentages of survival of all replicates of each sample.
(TIF)

S4 Fig. Identification of histidine kinase (*hk*) mutants of *S. pneumoniae* displaying normal intracellular survival in pneumocytes. A549 cells were infected with different *hk* mutants and its intracellular survival capacity was determined as described for non-virus infected cells in the Fig 1 legend, and these results were compared with those obtained for the *wt* strain. Green bars and blue bars correspond to 2 h and 4 h of incubation after antibiotic treatment, respectively.
(TIF)

S5 Fig. SirRH controls the acidic stress response of *S. pneumoniae* in pneumocytes. Raw data corresponding to the intracellular survival of the *wt*, Δ*sirR*, $\Delta atpC^{A49T}$ strains in A549 cells shown in Fig 2B, which were either infected with IAV or treated with 100 nM Bafilomycin A1, and compared with non-treated A549 cells. We represented CFU counting per well at time 0 h and 2 h, white bars correspond to CFU at 0 h and gray bars to CFU to 2h. Values represent mean ± SD. In the upper-table are represented the values of all replicates of each sample. In the bottom-table are represented the values of all replicates of each sample.
(TIF)

S6 Fig. Treatment with Bafilomycin A1 does not impair the pneumococcal growth. The *wt*, Δ*sirR*, Δ*clpL*, and Δ*psaB* strains were grown at 37˚C for 3 h in both BHI and BHI containing 100 nM Bafilomycin A1 (100nM). We counted CFU at 0h and 3h post-treatment. For these

strains, we observed no significant difference in their growth curves when bacteria cells were treated with Bafilomycin A1 and compared with non-treated pneumococci. The blue lines and circles correspond to control, and green lines and squares correspond to Bafilomycin A1-treatment conditions. Values represent the mean ± SD. Statistical significance was calculated by Student's t-test.
(TIF)

S7 Fig. SirRH controls the oxidative stress response of *S. pneumoniae* in pneumocytes. Raw data corresponding to the intracellular survival of the Δ*sirR*, *ΔsodA* and *wt* strains in A549 cells shown in Fig 3B, which were either infected with IAV or treated with 5 mM NAC. We represented CFU counting per well at time 0 h and 2 h, white bars correspond to CFU at 0h and green bars to CFU to 2h. Values represent mean ± SD. In the upper-table are represented the values of all replicates of each sample. In the bottom-table are represented the percentages of survival of all replicates of each sample.
(TIF)

S8 Fig. Confirmation of the IAV-induced ROS production in A549 cells. (A) Representative flow cytometry histogram showing results of H_2DCF-DA staining (a measurement of ROS levels) of IAV-infected A549 cells or mock-A549 cells. (B) Bar graph depicting results of IAV-infected A549 cells compared with non-infected cells. Data are representative of at least three independent experiments.
(TIF)

S9 Fig. A general scheme of the IAV/*S. pneumoniae* coinfection model in eukaryotic cells.
(TIF)

S10 Fig. Treatment with NAC does not impair the pneumococcal growth. The *wt*, *ΔsirR*, *ΔclpL*, and *ΔpsaB* strains were grown at 37˚C for 3 h in both BHI and BHI containing 5 mM N-acetyl-L-cysteine (NAC). We counted CFU at 0h and 3h post-treatment. For all the strains, we observed no significant difference in growth curves between control and NAC-treatment condition. The blue lines and circles correspond to control, and green lines and squares correspond to NAC-treatment conditions. Values represent the mean ± SD. Statistical significance was calculated by Student´s t-test.
(TIF)

S11 Fig. SirR is a global regulator that controls gene expression during the stress response. (A) Gene expression scatter plot in samples obtained from the *wt* strain and the Δ*sirR* mutants, with the *x*-axis representing the gene expression values for the control condition (*wt*) and the *y*-axis representing those for the treated condition (Δ*sirR*). Each black dot represents a significant single transcript, with the vertical position of each gene representing its expression level in the experimental conditions and the horizontal one representing its control strength. Thus, genes that fall above the diagonal are over-expressed whereas genes that fall below the diagonal are under-expressed as compared to their median expression levels in the experimental groups. (B) Volcano plot of gene expression in *wt* vs Δ*sirR* samples measured by RNAseq. The *y*-axis represents the mean expression value of the $\log_{10}$ (*p*-value), while the *x*-axis displays the $\log_2$ fold change value. Black dots represent genes with an expression 2-fold higher in the Δ*sirR* mutant relative to strain *wt* with a p-value < 0.05, with red dots signifying genes with an expression 2-fold lower in the Δ*sirR* mutant, which are relative to strain *wt* with a $p < 0.05$.
(TIF)

S12 Fig. Identification of the pneumococcal 78-kDa ClpL chaperone expressed under acidic conditions. (A) SDS-PAGE analysis of protein extracts obtained from the *wt* cells grew

at slightly alkaline (pH 7.8) or acidic (pH 5.9) culture media. The protein band subjected to N-terminal sequencing is indicated by an arrow. (B) The N-terminal sequence obtained by Edman degradation were analyzed by tryptic digestion and HLPC-protein sequencer. The m/z values of ions matching peptides derived from the 78-kDa protein band are indicated by numbers. The amino acids sequences corresponding to pick 8 (11 amino acids) and pick 12 (14 amino acids) corresponded to the ClpL chaperone, according to the R6 pneumococcal genome (https://www.uniprot.org/ proteomes/UP000000586). (C) Transcription levels of the *clpL* gene increased in cells exposed to acidic pH. The *wt* cells were grown in BHI/pH 7.8 to the mid-exponential phase and resuspended in ABM/pH 5.9, and total RNA was extracted at 1 h. The fold change in gene expression was measured by quantitative real-time PCR and calculated using the 2–ΔΔCT method. The *gyrA* gene was used as the internal control. Error bars indicate the standard deviation of the mean. INSTAT software was used to perform Dunnet's statistical comparison test for each strain. References: $^{**}p< 0.01$; $^{***}p< 0.001$.
(TIF)

S13 Fig. ClpL and PsaB are involved in the pneumococcal stress response needed for the viral-bacterial synergism. (A) Raw data corresponding to the intracellular survival assays shown in Fig 6E for the *wt*, Δ*clpL*, Δ*psaB* and Δ*sirR* strains, with either bacterial infection, IAV/bacterial coinfection, or bacterial infection with a 100 nM Bafilomycin A1 treatment. We represented CFU counting per well at time 0 h and 2 h, white bars correspond to CFU at 0h and grey bars to CFU to 2 h. Values represent mean ± SD. In the upper-table are represented the values of all replicates of each sample. In the bottom-table are represented the percentages of survival of all replicates of each sample. (B) Raw data corresponding to the intracellular survival assays for the *wt*, Δ*clpL*, Δ*psaB* and Δ*sirR* strains, with either bacterial infection, IAV/bacterial coinfection, or bacterial infection with a 5 mM NAC treatment shown in Fig 6E. We represented CFU counting per well at time 0 h and 2 h, white bars correspond to CFU at 0h and grey bars to CFU to 2h. Values represent mean ± SD. In the upper-table are represented the values of all replicates of each sample. In the bottom-table are represented the percentages of survival of all replicates of each sample.
(TIF)

S14 Fig. The double Δ*clpL*-Δ*psaB* mutant is susceptible to acidified media and to H_2O_2. (A) The *wt* and Δ*clpL*-Δ*psaB* cells were grown in BHI at 37˚C until an OD_{620nm} 0.3, and then incubated in ABM medium at pH 4.8 for 1 h at 37˚C. Viable cells were assessed by spreading dilutions in BHI-blood-agar plates and incubating these at 37˚C for 16 h. (B) The *wt* and Δ*clpL*-Δ*psaB* cells were grown in BHI and then exposed at BHI medium containing 20 mM H_2O_2 for 2 h. After that, viable cells were determined by spreading dilutions in BHI-blood-agar plates and incubating these at 37˚C for 16 h. Data are representative of at least three independent experiments. Values represent mean ± SD Statistical significance was calculated by Student's t-test, $p<0.001$ (***).
(TIF)

S15 Fig. Manganese pre-treatment of *S. pneumoniae* raises intracellular bacterial survival in a dose-dependent manner. The *wt* strain was cultivated in BHI with different concentrations of $MnSO_4$ (1, 30 and 100 μM) until reaching an OD_{600nm} 0.3. Then, A549 cells were infected with these Mn-pretreated bacterial cells, and the intracellular survival for each condition was measured. White bar corresponds to control and the shades of gray correspond to different concentrations of Mn^{2+}. One representative experiment of three independent assays is shown. Values represent the mean ± SD. Statistical significance was calculated by one-way

ANOVA, followed by Post Hoc Test Tukey, $p<0.05$ (*).
(TIF)

S16 Fig. IAV and *S. pneumoniae* infection and superinfection induce autophagy in A549 cells. (A) LC3-II levels are induced by superinfection with IAV and *S. pneumoniae*. A549 cells were infected with IAV (MOI 10), *S. pneumoniae* (MOI 30) and coinfected as described in the Fig 1A legend. As controls, A549 cells were also treated with inducers (Rapamycin) and inhibitors (Bafilomycin A1) of the autophagy process. Cell lysates were subjected to Western blot analysis using anti-LC3-II, anti-beta-actin antibodies with data being representative of at least three independent experiments. (B) Quantification of the LC3-II level in western blot: bar graphs represent LC3-II relative intensity (LC3-II/β-actin) with data being representative of at least three independent experiments.
(TIF)

S17 Fig. Formation of the puncta of mKate2-hLC3 indicated autophagy induction during IAV, the pneumococcal *wt* and *ΔsirR* strains, and superinfection. The A549 cells were transfected with the mKate2-hLC3 plasmids for 24 hours, and followed by either IAV, individual pneumococcal strains (*wt* or Δ*sirR*), or superinfection with each strain. The far-red (mKate2) fluorescence in the cells was monitored using an Olympus FluoView FV1000 confocal laser scanning microscope.
(TIF)

S18 Fig. Formation of the puncta of mKate2-hLC3 indicated autophagy induction during IAV, the pneumococcal *ΔpsaB* and *ΔclpL* mutants, and superinfection. The A549 cells were transfected with the mKate2-hLC3 plasmids for 24 hours, and followed by either IAV, individual pneumococcal strains (*ΔclpL* or *ΔpsaB*), or superinfection with each strain. These assays were processed at the same time that those shown in the S17 Fig. The far-red (mKate2) fluorescence in the cells was monitored using an Olympus FluoView FV1000 confocal laser scanning microscope.
(TIF)

S19 Fig. The viral-bacterial synergism is dependent on autophagic-proficient cells. Raw data corresponding to the intracellular survival assays shown in Fig 7A and 7B for the MEF *wt* (A) and MEF *atg5-KO* cells (B), with either bacterial infection or IAV/bacterial coinfection. We represented CFU counting per well at time 0 h and 2 h, white bars correspond to CFU at 0h and grey bars to CFU to 2 h. Values represent mean ± SD. In the upper-table are represented the values of all replicates of each sample. In the bottom-table are represented the percentages of survival of all replicates of each sample.
(TIF)

S1 Table. Bacterial strains and plasmids used in this work.
(DOCX)

S2 Table. List of SirR-regulated genes as determined by RNAseq analysis between the *ΔsirR* mutant and the *wt* strain.
(XLS)

S3 Table. List of differentially expressed proteins at pH 5.9 as determined by proteomic analysis between the *ΔsirR* mutant and the *wt* strain.
(XLSX)

S4 Table. List of differentially expressed proteins at pH 7.0 as determined by proteomic analysis between the *ΔsirR* mutant and the *wt* strain.
(XLSX)

S5 Table. List of primers used in this work.
(DOCX)

Acknowledgments

We thank Gabriela Furlan, Laura Gatica, Paula Abadie, Pilar Crespo, Alejandra Romero, Luciana Reyna (CIBICI-CONICET), Carlos Mas (CIQUIBIC-CONICET), María Pía Valacco and Ricardo Neme Tauil (CEQUIBIEM-CONICET) for their skillful technical assistance. We also thank Dr. Silvia Moreno (CEQUIBIEM-CONICET) for her contribution in the proteomic analysis. We thank Dr. Noboru Mizushima (Department of Biochemistry and Molecular Biology, The University of Tokyo, Japan) for the kind gift of MEF *atg5-KO* and MEF *wt*. We thank Dr. Beate Illek (University of California-San Francisco, USA) for the 16HBE14o- cell line, which was originated by Dr. Dieter Gruenert (University of California-San Francisco, USA). A special acknowledgment to Dr. Analia Trevani and Dr. Florencia Sabbione (Laboratorio de Inmunidad Innata, IMEX-CONICET, Academia Nacional de Medicina, Buenos Aires Argentina) for their help to obtain the 16HBE14o- cell line. We especially thank Dr. Alex Saka (CIBICI-CONICET, Facultad de Ciencias Quimicas, Universidad Nacional de Cordoba, Argentina) for valuable discussions while writing our responses to the referees and for editing the manuscript.

Author Contributions

Conceptualization: Nicolás M. Reinoso-Vizcaíno, Melina B. Cian, Paulo R. Cortes, Nadia B. Olivero, Mirelys Hernandez-Morfa, Germán E. Piñas, Daniel R. Perez, José Echenique.

Formal analysis: Nicolás M. Reinoso-Vizcaíno, Melina B. Cian, Paulo R. Cortes, Chandan Badapanda, Ankita Rathore, José Echenique.

Funding acquisition: Daniel R. Perez, José Echenique.

Investigation: Nicolás M. Reinoso-Vizcaíno, Melina B. Cian, Paulo R. Cortes, Nadia B. Olivero, Mirelys Hernandez-Morfa, Germán E. Piñas, Chandan Badapanda, Ankita Rathore, Daniel R. Perez, José Echenique.

Methodology: Nicolás M. Reinoso-Vizcaíno, Melina B. Cian, Chandan Badapanda, Ankita Rathore, Daniel R. Perez, José Echenique.

Project administration: José Echenique.

Supervision: José Echenique.

Validation: Nicolás M. Reinoso-Vizcaíno, Melina B. Cian, Paulo R. Cortes, Nadia B. Olivero, Mirelys Hernandez-Morfa, Chandan Badapanda, Ankita Rathore.

Visualization: Nicolás M. Reinoso-Vizcaíno, Melina B. Cian, Paulo R. Cortes, Nadia B. Olivero, José Echenique.

Writing – original draft: Nicolás M. Reinoso-Vizcaíno, Melina B. Cian, Paulo R. Cortes, Nadia B. Olivero, Chandan Badapanda, Ankita Rathore, Daniel R. Perez, José Echenique.

Writing – review & editing: Nicolás M. Reinoso-Vizcaíno, Melina B. Cian, Paulo R. Cortes, Daniel R. Perez, José Echenique.

References

1. Klein EY, Monteforte B, Gupta A, Jiang W, May L, Hsieh YH, et al. The frequency of influenza and bacterial coinfection: a systematic review and meta-analysis. Influenza and other respiratory viruses. 2016; 10(5):394–403. https://doi.org/10.1111/irv.12398 PMID: 27232677; PubMed Central PMCID: PMC4947938.
2. Smith AM, McCullers JA. Secondary bacterial infections in influenza virus infection pathogenesis. Current topics in microbiology and immunology. 2014; 385:327–56. https://doi.org/10.1007/82_2014_394 PMID: 25027822.
3. Joseph C, Togawa Y, Shindo N. Bacterial and viral infections associated with influenza. Influenza and other respiratory viruses. 2013; 7 Suppl 2:105–13. https://doi.org/10.1111/irv.12089 PMID: 24034494; PubMed Central PMCID: PMC5909385.
4. Brundage JF, Shanks GD. Deaths from bacterial pneumonia during 1918–19 influenza pandemic. Emerging infectious diseases. 2008; 14(8):1193–9. https://doi.org/10.3201/eid1408.071313 PMID: 18680641; PubMed Central PMCID: PMC2600384.
5. Morens DM, Taubenberger JK, Fauci AS. Predominant role of bacterial pneumonia as a cause of death in pandemic influenza: implications for pandemic influenza preparedness. The Journal of infectious diseases. 2008; 198(7):962–70. https://doi.org/10.1086/591708 PMID: 18710327; PubMed Central PMCID: PMC2599911.
6. Kim L, McGee L, Tomczyk S, Beall B. Biological and Epidemiological Features of Antibiotic-Resistant *Streptococcus pneumoniae* in Pre- and Post-Conjugate Vaccine Eras: a United States Perspective. Clinical microbiology reviews. 2016; 29(3):525–52. https://doi.org/10.1128/CMR.00058-15 PMID: 27076637; PubMed Central PMCID: PMC4861989.
7. Dawood FS, Iuliano AD, Reed C, Meltzer MI, Shay DK, Cheng PY, et al. Estimated global mortality associated with the first 12 months of 2009 pandemic influenza A H1N1 virus circulation: a modelling study. The Lancet Infectious diseases. 2012; 12(9):687–95. https://doi.org/10.1016/S1473-3099(12)70121-4 PMID: 22738893.
8. Chertow DS, Memoli MJ. Bacterial coinfection in influenza: a grand rounds review. Jama. 2013; 309 (3):275–82. https://doi.org/10.1001/jama.2012.194139 PMID: 23321766.
9. McCullers JA. Insights into the interaction between influenza virus and pneumococcus. Clinical microbiology reviews. 2006; 19(3):571–82. https://doi.org/10.1128/CMR.00058-05 PMID: 16847087.
10. McCullers JA. The co-pathogenesis of influenza viruses with bacteria in the lung. Nature reviews Microbiology. 2014; 12(4):252–62. https://doi.org/10.1038/nrmicro3231 PMID: 24590244.
11. McNamee LA, Harmsen AG. Both influenza-induced neutrophil dysfunction and neutrophil-independent mechanisms contribute to increased susceptibility to a secondary *Streptococcus pneumoniae* infection. Infection and immunity. 2006; 74(12):6707–21. https://doi.org/10.1128/IAI.00789-06 PMID: 16982840.
12. Abramson JS, Giebink GS, Mills EL, Quie PG. Polymorphonuclear leukocyte dysfunction during influenza virus infection in chinchillas. The Journal of infectious diseases. 1981; 143(6):836–45. https://doi.org/10.1093/infdis/143.6.836 PMID: 7252265.
13. Ercoli G, Fernandes VE, Chung WY, Wanford JJ, Thomson S, Bayliss CD, et al. Intracellular replication of *Streptococcus pneumoniae* inside splenic macrophages serves as a reservoir for septicaemia. Nature microbiology. 2018; 3(5):600–10. https://doi.org/10.1038/s41564-018-0147-1 PMID: 29662129; PubMed Central PMCID: PMC6207342.
14. Ogawa M, Matsuda R, Takada N, Tomokiyo M, Yamamoto S, Shizukusihi S, et al. Molecular mechanisms of *Streptococcus pneumoniae*-targeted autophagy via pneumolysin, Golgi-resident Rab41, and Nedd4-1-mediated K63-linked ubiquitination. Cellular microbiology. 2018; 20(8):e12846. https://doi.org/10.1111/cmi.12846 PMID: 29582580.
15. Cortes PR, Pinas GE, Cian MB, Yandar N, Echenique J. Stress-triggered signaling affecting survival or suicide of *Streptococcus pneumoniae*. Int J Med Microbiol. 2015; 305(1):157–69. https://doi.org/10.1016/j.ijmm.2014.12.002 PMID: 25543170.
16. Pinas GE, Reinoso-Vizcaino NM, Yandar Barahona NY, Cortes PR, Duran R, Badapanda C, et al. Crosstalk between the serine/threonine kinase StkP and the response regulator ComE controls the stress response and intracellular survival of *Streptococcus pneumoniae*. PLoS Pathog. 2018; 14(6): e1007118. https://doi.org/10.1371/journal.ppat.1007118 PMID: 29883472; PubMed Central PMCID: PMC6010298.
17. Kilbourne ED. Future influenza vaccines and the use of genetic recombinants. Bulletin of the World Health Organization. 1969; 41(3):643–5. PMID: 5309489; PubMed Central PMCID: PMC2427719.
18. Lefevre JC, Claverys JP, Sicard AM. Donor deoxyribonucleic acid length and marker effect in pneumococcal transformation. Journal of bacteriology. 1979; 138(1):80–6. https://doi.org/10.1128/JB.138.1.80-86.1979 PMID: 35523; PubMed Central PMCID: PMC218240.

19. Avery OT, Macleod CM, McCarty M. Studies on the Chemical Nature of the Substance Inducing Transformation of Pneumococcal Types: Induction of Transformation by a Desoxyribonucleic Acid Fraction Isolated from Pneumococcus Type Iii. The Journal of experimental medicine. 1944; 79(2):137–58. https://doi.org/10.1084/jem.79.2.137 PMID: 19871359; PubMed Central PMCID: PMC2135445.

20. Ottolenghi E, Hotchkiss RD. Appearance of genetic transforming activity in pneumococcal cultures. Science. 1960; 132(3435):1257–8. PMID: 13731684.

21. Gill JR, Sheng ZM, Ely SF, Guinee DG, Beasley MB, Suh J, et al. Pulmonary pathologic findings of fatal 2009 pandemic influenza A/H1N1 viral infections. Archives of pathology & laboratory medicine. 2010; 134(2):235–43. https://doi.org/10.1043/1543-2165-134.2.235 PMID: 20121613; PubMed Central PMCID: PMC2819217.

22. Cozens AL, Yezzi MJ, Kunzelmann K, Ohrui T, Chin L, Eng K, et al. CFTR expression and chloride secretion in polarized immortal human bronchial epithelial cells. American journal of respiratory cell and molecular biology. 1994; 10(1):38–47. https://doi.org/10.1165/ajrcmb.10.1.7507342 PMID: 7507342.

23. Hava DL, Camilli A. Large-scale identification of serotype 4 *Streptococcus pneumoniae* virulence factors. Molecular microbiology. 2002; 45(5):1389–406. PMID: 12207705; PubMed Central PMCID: PMC2788772.

24. Throup JP, Koretke KK, Bryant AP, Ingraham KA, Chalker AF, Ge Y, et al. A genomic analysis of two-component signal transduction in *Streptococcus pneumoniae*. Molecular microbiology. 2000; 35 (3):566–76. https://doi.org/10.1046/j.1365-2958.2000.01725.x PMID: 10672179.

25. Trihn M, Ge X, Dobson A, Kitten T, Munro CL, Xu P. Two-component system response regulators involved in virulence of *Streptococcus pneumoniae* TIGR4 in infective endocarditis. PloS one. 2013; 8(1):e54320. https://doi.org/10.1371/journal.pone.0054320 PMID: 23342132; PubMed Central PMCID: PMC3546988.

26. Sung CK, Li H, Claverys JP, Morrison DA. An rpsL cassette, janus, for gene replacement through negative selection in *Streptococcus pneumoniae*. Applied and environmental microbiology. 2001; 67 (11):5190–6. https://doi.org/10.1128/AEM.67.11.5190-5196.2001 PMID: 11679344; PubMed Central PMCID: PMC93289.

27. Jacob-Dubuisson F, Mechaly A, Betton JM, Antoine R. Structural insights into the signalling mechanisms of two-component systems. Nature reviews Microbiology. 2018; 16(10):585–93. https://doi.org/10.1038/s41579-018-0055-7 PMID: 30008469.

28. Albarracin Orio AG, Cortes PR, Tregnaghi M, Pinas GE, Argentinean Network Pneumococcus Study G, Echenique JR. A new serotype 14 variant of the pneumococcal Spain9V-3 international clone detected in the central region of Argentina. Journal of medical microbiology. 2008; 57(Pt 8):992–9. https://doi.org/10.1099/jmm.0.2008/000505-0 PMID: 18628501.

29. Gagliardi S, Rees M, Farina C. Chemistry and structure activity relationships of bafilomycin A1, a potent and selective inhibitor of the vacuolar H^+-ATPase. Current medicinal chemistry. 1999; 6(12):1197–212. PMID: 10519916.

30. Surve MV, Bhutda S, Datey A, Anil A, Rawat S, Pushpakaran A, et al. Heterogeneity in pneumolysin expression governs the fate of *Streptococcus pneumoniae* during blood-brain barrier trafficking. PLoS pathogens. 2018; 14(7):e1007168. https://doi.org/10.1371/journal.ppat.1007168 PMID: 30011336; PubMed Central PMCID: PMC6062133.

31. Gannage M, Dormann D, Albrecht R, Dengjel J, Torossi T, Ramer PC, et al. Matrix protein 2 of influenza A virus blocks autophagosome fusion with lysosomes. Cell host & microbe. 2009; 6(4):367–80. https://doi.org/10.1016/j.chom.2009.09.005 PMID: 19837376; PubMed Central PMCID: PMC2774833.

32. McCluskey J, Hinds J, Husain S, Witney A, Mitchell TJ. A two-component system that controls the expression of pneumococcal surface antigen A (PsaA) and regulates virulence and resistance to oxidative stress in *Streptococcus pneumoniae*. Molecular microbiology. 2004; 51(6):1661–75. https://doi.org/10.1111/j.1365-2958.2003.03917.x PMID: 15009893.

33. Yesilkaya H, Kadioglu A, Gingles N, Alexander JE, Mitchell TJ, Andrew PW. Role of manganese-containing superoxide dismutase in oxidative stress and virulence of *Streptococcus pneumoniae*. Infection and immunity. 2000; 68(5):2819–26. https://doi.org/10.1128/iai.68.5.2819-2826.2000 PMID: 10768978; PubMed Central PMCID: PMC97493.

34. McAllister LJ, Tseng HJ, Ogunniyi AD, Jennings MP, McEwan AG, Paton JC. Molecular analysis of the psa permease complex of *Streptococcus pneumoniae*. Molecular microbiology. 2004; 53(3):889–901. https://doi.org/10.1111/j.1365-2958.2004.04164.x PMID: 15255900.

35. Khomich OA, Kochetkov SN, Bartosch B, Ivanov AV. Redox Biology of Respiratory Viral Infections. Viruses. 2018; 10(8). https://doi.org/10.3390/v10080392 PMID: 30049972; PubMed Central PMCID: PMC6115776.

36. Komaravelli N, Casola A. Respiratory Viral Infections and Subversion of Cellular Antioxidant Defenses. Journal of pharmacogenomics & pharmacoproteomics. 2014; 5(4). https://doi.org/10.4172/2153-0645.1000141 PMID: 25584194; PubMed Central PMCID: PMC4288774.

37. Paul M, Thushara RM, Jagadish S, Zakai UI, West R, Kemparaju K, et al. Novel sila-amide derivatives of N-acetylcysteine protects platelets from oxidative stress-induced apoptosis. Journal of thrombosis and thrombolysis. 2017; 43(2):209–16. https://doi.org/10.1007/s11239-016-1450-4 PMID: 27804000.

38. Park SS, Kwon HY, Tran TD, Choi MH, Jung SH, Lee S, et al. ClpL is a chaperone without auxiliary factors. The FEBS journal. 2015; 282(8):1352–67. https://doi.org/10.1111/febs.13228 PMID: 25662392.

39. Choi IH, Shim JH, Kim SW, Kim SN, Pyo SN, Rhee DK. Limited stress response in *Streptococcus pneumoniae*. Microbiology and immunology. 1999; 43(8):807–12. https://doi.org/10.1111/j.1348-0421.1999.tb02474.x PMID: 10524800.

40. Filipe SR, Tomasz A. Inhibition of the expression of penicillin resistance in *Streptococcus pneumoniae* by inactivation of cell wall muropeptide branching genes. Proceedings of the National Academy of Sciences of the United States of America. 2000; 97(9):4891–6. https://doi.org/10.1073/pnas.080067697 PMID: 10759563; PubMed Central PMCID: PMC18328.

41. Jiang YL, Jin H, Yang HB, Zhao RL, Wang S, Chen Y, et al. Defining the enzymatic pathway for polymorphic O-glycosylation of the pneumococcal serine-rich repeat protein PsrP. The Journal of biological chemistry. 2017; 292(15):6213–24. https://doi.org/10.1074/jbc.M116.770446 PMID: 28246170; PubMed Central PMCID: PMC5391752.

42. Horsburgh MJ, Foster TJ, Barth PT, Coggins JR. Chorismate synthase from *Staphylococcus aureus*. Microbiology. 1996; 142 (Pt 10):2943–50. https://doi.org/10.1099/13500872-142-10-2943 PMID: 8885411.

43. Hua CZ, Howard A, Malley R, Lu YJ. Effect of nonheme iron-containing ferritin Dpr in the stress response and virulence of pneumococci. Infection and immunity. 2014; 82(9):3939–47. https://doi.org/10.1128/IAI.01829-14 PMID: 25001605; PubMed Central PMCID: PMC4187797.

44. Jacob C, Kriznik A, Boschi-Muller S, Branlant G. Thioredoxin 2 from *Escherichia coli* is not involved in vivo in the recycling process of methionine sulfoxide reductase activities. FEBS letters. 2011; 585 (12):1905–9. https://doi.org/10.1016/j.febslet.2011.04.070 PMID: 21570393.

45. Kim SN, Kim SW, Pyo SN, Rhee DK. Molecular cloning and characterization of *groESL* operon in *Streptococcus pneumoniae*. Molecules and cells. 2001; 11(3):360–8. PMID: 11459227.

46. Dreux N, del Mar Cendra M, Massier S, Darfeuille-Michaud A, Barnich N, Torrents E. Ribonucleotide reductase NrdR as a novel regulator for motility and chemotaxis during adherent-invasive *Escherichia coli* infection. Infection and immunity. 2015; 83(4):1305–17. https://doi.org/10.1128/IAI.02772-14 PMID: 25605769; PubMed Central PMCID: PMC4363436.

47. Law AH, Lee DC, Leon TY, Lau AS. Role for autophagy in cellular response to influenza virus infection. Hong Kong medical journal, Xianggang yi xue za zhi. 2014; 20 Suppl 6:20–4. PMID: 25482966.

48. Li P, Shi J, He Q, Hu Q, Wang YY, Zhang LJ, et al. *Streptococcus pneumoniae* induces autophagy through the inhibition of the PI3K-I/Akt/mTOR pathway and ROS hypergeneration in A549 cells. PloS one. 2015; 10(3):e0122753. https://doi.org/10.1371/journal.pone.0122753 PMID: 25803050; PubMed Central PMCID: PMC4372526.

49. Yamamoto A, Tagawa Y, Yoshimori T, Moriyama Y, Masaki R, Tashiro Y. Bafilomycin A1 prevents maturation of autophagic vacuoles by inhibiting fusion between autophagosomes and lysosomes in rat hepatoma cell line, H-4-II-E cells. Cell structure and function. 1998; 23(1):33–42. https://doi.org/10.1247/csf.23.33 PMID: 9639028.

50. Kepp O, Senovilla L, Vitale I, Vacchelli E, Adjemian S, Agostinis P, et al. Consensus guidelines for the detection of immunogenic cell death. Oncoimmunology. 2014; 3(9):e955691. https://doi.org/10.4161/21624011.2014.955691 PMID: 25941621; PubMed Central PMCID: PMC4292729.

51. Zhou Z, Jiang X, Liu D, Fan Z, Hu X, Yan J, et al. Autophagy is involved in influenza A virus replication. Autophagy. 2009; 5(3):321–8. https://doi.org/10.4161/auto.5.3.7406 PMID: 19066474.

52. Tanida I, Ueno T, Uchiyama Y. Use of pHlurorin-mKate2-human LC3 to Monitor Autophagic Responses. Methods in enzymology. 2017; 587:87–96. https://doi.org/10.1016/bs.mie.2016.09.054 PMID: 28253978.

53. Kuma A, Hatano M, Matsui M, Yamamoto A, Nakaya H, Yoshimori T, et al. The role of autophagy during the early neonatal starvation period. Nature. 2004; 432(7020):1032–6. https://doi.org/10.1038/nature03029 PMID: 15525940.

54. Pasqua M, Grossi M, Scinicariello S, Aussel L, Barras F, Colonna B, et al. The MFS efflux pump EmrKY contributes to the survival of Shigella within macrophages. Scientific reports. 2019; 9(1):2906. https://doi.org/10.1038/s41598-019-39749-3 PMID: 30814604; PubMed Central PMCID: PMC6393483.

55. Pardo-Este C, Hidalgo AA, Aguirre C, Inostroza A, Briones AC, Cabezas CE, et al. Correction: The ArcAB two-component regulatory system promotes resistance to reactive oxygen species and systemic infection by *Salmonella Typhimurium*. PloS one. 2019; 14(3):e0214634. https://doi.org/10.1371/journal.pone.0214634 PMID: 30913267.

56. Bourret TJ, Liu L, Shaw JA, Husain M, Vazquez-Torres A. Magnesium homeostasis protects *Salmonella* against nitrooxidative stress. Scientific reports. 2017; 7(1):15083. https://doi.org/10.1038/s41598-017-15445-y PMID: 29118452; PubMed Central PMCID: PMC5678156.

57. Kenney LJ. The role of acid stress in *Salmonella pathogenesis*. Current opinion in microbiology. 2018; 47:45–51. https://doi.org/10.1016/j.mib.2018.11.006 PMID: 30529007.

58. James KL, Mogen AB, Brandwein JN, Orsini SS, Ridder MJ, Markiewicz MA, et al. Interplay of Nitric Oxide Synthase (NOS) and SrrAB in Modulation of *Staphylococcus aureus* Metabolism and Virulence. Infection and immunity. 2019; 87(2). https://doi.org/10.1128/IAI.00570-18 PMID: 30420450; PubMed Central PMCID: PMC6346124.

59. Flannagan RS, Kuiack RC, McGavin MJ, Heinrichs DE. *Staphylococcus aureus* Uses the GraXRS Regulatory System To Sense and Adapt to the Acidified Phagolysosome in Macrophages. mBio. 2018; 9 (4). https://doi.org/10.1128/mBio.01143-18 PMID: 30018109; PubMed Central PMCID: PMC6050959.

60. Zhuge X, Sun Y, Xue F, Tang F, Ren J, Li D, et al. A Novel PhoP/PhoQ Regulation Pathway Modulates the Survival of Extraintestinal Pathogenic *Escherichia coli* in Macrophages. Frontiers in immunology. 2018; 9:788. https://doi.org/10.3389/fimmu.2018.00788 PMID: 29719540; PubMed Central PMCID: PMC5913352.

61. Altamirano-Silva P, Meza-Torres J, Castillo-Zeledon A, Ruiz-Villalobos N, Zuniga-Pereira AM, Chacon-Diaz C, et al. *Brucella abortus* Senses the Intracellular Environment through the BvrR/BvrS Two-Component System, Which Allows B. abortus To Adapt to Its Replicative Niche. Infection and immunity. 2018; 86(4). https://doi.org/10.1128/IAI.00713-17 PMID: 29378792; PubMed Central PMCID: PMC5865028.

62. Mishra AK, Yabaji SM, Dubey RK, Dhamija E, Srivastava KK. Dual phosphorylation in response regulator protein PrrA is crucial for intracellular survival of mycobacteria consequent upon transcriptional activation. The Biochemical journal. 2017; 474(24):4119–36. https://doi.org/10.1042/BCJ20170596 PMID: 29101285.

63. Paterson GK, Blue CE, Mitchell TJ. Role of two-component systems in the virulence of *Streptococcus pneumoniae*. Journal of medical microbiology. 2006; 55(Pt 4):355–63. https://doi.org/10.1099/jmm.0.46423-0 PMID: 16533981.

64. Gomez-Mejia A, Gamez G, Hammerschmidt S. *Streptococcus pneumoniae* two-component regulatory systems: The interplay of the pneumococcus with its environment. International journal of medical microbiology: IJMM. 2018; 308(6):722–37. https://doi.org/10.1016/j.ijmm.2017.11.012 PMID: 29221986.

65. Kwon HY, Kim SW, Choi MH, Ogunniyi AD, Paton JC, Park SH, et al. Effect of heat shock and mutations in ClpL and ClpP on virulence gene expression in *Streptococcus pneumoniae*. Infection and immunity. 2003; 71(7):3757–65. https://doi.org/10.1128/iai.71.7.3757-3765.2003 PMID: 12819057; PubMed Central PMCID: PMC162022.

66. Le NT, Jeong HY, Kwon HY, Ogunniyi AD, Paton JC, Pyo SN, et al. Modulation of adherence, invasion, and tumor necrosis factor alpha secretion during the early stages of infection by *Streptococcus pneumoniae* ClpL. Infection and immunity. 2007; 75(6):2996–3005. https://doi.org/10.1128/IAI.01716-06 PMID: 17403879; PubMed Central PMCID: PMC1932908.

67. Nguyen CT, Le NT, Tran TD, Kim EH, Park SS, Luong TT, et al. *Streptococcus pneumoniae* ClpL modulates adherence to A549 human lung cells through Rap1/Rac1 activation. Infection and immunity. 2014; 82(9):3802–10. https://doi.org/10.1128/IAI.02012-14 PMID: 24980975; PubMed Central PMCID: PMC4187815.

68. Tran TD, Kwon HY, Kim EH, Kim KW, Briles DE, Pyo S, et al. Decrease in penicillin susceptibility due to heat shock protein ClpL in *Streptococcus pneumoniae*. Antimicrobial agents and chemotherapy. 2011; 55(6):2714–28. https://doi.org/10.1128/AAC.01383-10 PMID: 21422206; PubMed Central PMCID: PMC3101445.

69. Len AC, Harty DW, Jacques NA. Proteome analysis of *Streptococcus mutans* metabolic phenotype during acid tolerance. Microbiology. 2004; 150(Pt 5):1353–66. https://doi.org/10.1099/mic.0.26888-0 PMID: 15133097.

70. Tao L, Biswas I. ClpL is required for folding of CtsR in *Streptococcus mutans*. Journal of bacteriology. 2013; 195(3):576–84. https://doi.org/10.1128/JB.01743-12 PMID: 23204456; PubMed Central PMCID: PMC3554016.

71. Novak R, Braun JS, Charpentier E, Tuomanen E. Penicillin tolerance genes of *Streptococcus pneumoniae*: the ABC-type manganese permease complex Psa. Molecular microbiology. 1998; 29(5):1285–96. https://doi.org/10.1046/j.1365-2958.1998.01016.x PMID: 9767595.

72. Marra A, Lawson S, Asundi JS, Brigham D, Hromockyj AE. In vivo characterization of the psa genes from *Streptococcus pneumoniae* in multiple models of infection. Microbiology. 2002; 148(Pt 5):1483–91. https://doi.org/10.1099/00221287-148-5-1483 PMID: 11988523.

73. Johnston JW, Myers LE, Ochs MM, Benjamin WH Jr., Briles DE, Hollingshead SK. Lipoprotein PsaA in virulence of *Streptococcus pneumoniae*: surface accessibility and role in protection from superoxide. Infection and immunity. 2004; 72(10):5858–67. https://doi.org/10.1128/IAI.72.10.5858-5867.2004 PMID: 15385487; PubMed Central PMCID: PMC517531.

74. Kajfasz JK, Rivera-Ramos I, Abranches J, Martinez AR, Rosalen PL, Derr AM, et al. Two Spx proteins modulate stress tolerance, survival, and virulence in *Streptococcus mutans*. Journal of bacteriology. 2010; 192(10):2546–56. https://doi.org/10.1128/JB.00028-10 PMID: 20233935; PubMed Central PMCID: PMC2863552.

75. Chastanet A, Prudhomme M, Claverys JP, Msadek T. Regulation of *Streptococcus pneumoniae clp* genes and their role in competence development and stress survival. Journal of bacteriology. 2001; 183 (24):7295–307. https://doi.org/10.1128/JB.183.24.7295-7307.2001 PMID: 11717289; PubMed Central PMCID: PMC95579.

76. Kloosterman TG, Witwicki RM, van der Kooi-Pol MM, Bijlsma JJ, Kuipers OP. Opposite effects of Mn^{+2} and Zn^{+2} on PsaR-mediated expression of the virulence genes *pcpA*, *prtA*, and *psaBCA* of *Streptococcus pneumoniae*. Journal of bacteriology. 2008; 190(15):5382–93. https://doi.org/10.1128/JB.00307-08 PMID: 18515418; PubMed Central PMCID: PMC2493273.

77. Pyo CW, Shin N, Jung KI, Choi JH, Choi SY. Alteration of copper-zinc superoxide dismutase 1 expression by influenza A virus is correlated with virus replication. Biochemical and biophysical research communications. 2014; 450(1):711–6. https://doi.org/10.1016/j.bbrc.2014.06.037 PMID: 24946209.

78. Gennaris A, Collet JF. The 'captain of the men of death', *Streptococcus pneumoniae*, fights oxidative stress outside the 'city wall'. EMBO molecular medicine. 2013; 5(12):1798–800. https://doi.org/10.1002/emmm.201303482 PMID: 24293314; PubMed Central PMCID: PMC3914527.

79. Eijkelkamp BA, Morey JR, Ween MP, Ong CL, McEwan AG, Paton JC, et al. Extracellular zinc competitively inhibits manganese uptake and compromises oxidative stress management in *Streptococcus pneumoniae*. PloS one. 2014; 9(2):e89427. https://doi.org/10.1371/journal.pone.0089427 PMID: 24558498; PubMed Central PMCID: PMC3928430.

80. Turner AG, Ong CY, Walker MJ, Djoko KY, McEwan AG. Transition Metal Homeostasis in *Streptococcus pyogenes* and *Streptococcus pneumoniae*. Advances in microbial physiology. 2017; 70:123–91. https://doi.org/10.1016/bs.ampbs.2017.01.002 PMID: 28528647.

81. Albarracin Orio AG, Pinas GE, Cortes PR, Cian MB, Echenique J. Compensatory evolution of *pbp* mutations restores the fitness cost imposed by beta-lactam resistance in *Streptococcus pneumoniae*. PLoS pathogens. 2011; 7(2):e1002000. https://doi.org/10.1371/journal.ppat.1002000 PMID: 21379570; PubMed Central PMCID: PMC3040684.

82. Chockalingam AK, Hickman D, Pena L, Ye J, Ferrero A, Echenique JR, et al. Deletions in the neuraminidase stalk region of H2N2 and H9N2 avian influenza virus subtypes do not affect postinfluenza secondary bacterial pneumonia. Journal of virology. 2012; 86(7):3564–73. https://doi.org/10.1128/JVI.05809-11 PMID: 22278240; PubMed Central PMCID: PMC3302490.

83. Webster R, Cox, N., & Stohr, K. WHO manual on animal influenza diagnosis and surveillance. Retrieved from http://wwwwhoint/csr/resources/public. 2005.

84. Sabbione F, Keitelman IA, Iula L, Ferrero M, Giordano MN, Baldi P, et al. Neutrophil Extracellular Traps Stimulate Proinflammatory Responses in Human Airway Epithelial Cells. Journal of innate immunity. 2017; 9(4):387–402. https://doi.org/10.1159/000460293 PMID: 28467984; PubMed Central PMCID: PMC6738901.

85. Morelli L, Llovera R, Gonzalez SA, Affranchino JL, Prelli F, Frangione B, et al. Differential degradation of amyloid beta genetic variants associated with hereditary dementia or stroke by insulin-degrading enzyme. The Journal of biological chemistry. 2003; 278(26):23221–6. https://doi.org/10.1074/jbc.M300276200 PMID: 12695513.

86. Tyanova S, Temu T, Sinitcyn P, Carlson A, Hein MY, Geiger T, et al. The Perseus computational platform for comprehensive analysis of (prote)omics data. Nature methods. 2016; 13(9):731–40. https://doi.org/10.1038/nmeth.3901 PMID: 27348712.

87. Livak KJ, Schmittgen TD. Analysis of relative gene expression data using real-time quantitative PCR and the 2(-Delta Delta C(T)) Method. Methods. 2001; 25(4):402–8. https://doi.org/10.1006/meth.2001.1262 PMID: 11846609.

88. Mann B, van Opijnen T, Wang J, Obert C, Wang YD, Carter R, et al. Control of virulence by small RNAs in *Streptococcus pneumoniae*. PLoS pathogens. 2012; 8(7):e1002788. https://doi.org/10.1371/journal.ppat.1002788 PMID: 22807675; PubMed Central PMCID: PMC3395615.